was not different from that in control cells (**Figure 3a**). In addition, procollagen PHD2, a member of another prolyl 4-hydroxylase family, was also not influenced by pshPHD2 vector- or siRNA-induced PHD2 silencing (**Figure 3b** and **Supplementary Figure S4**). However, the mRNA levels of angiogenic growth factor genes, *i.e.*, VEGF, FGF2, and angiopoietin-1, were significantly increased (**Figure 3c–e**), while the expression level of PDGF-B was not altered (data not shown). These results indicate that the increase in VEGF, FGF2, and angiopoietin-1 induced by PHD2 silencing might be caused by the stabilization of HIF-1α rather than by the increase in HIF-1α mRNA expression.

Effect of PHD2 silencing on VEGF secretion

As shown in **Figure 4a**, the amount of VEGF secreted was significantly higher in PHD2-silenced cells than in control cells. Consistent with the higher suppressive effect of U6-pshPHD2-A, the level of VEGF secretion from cells transfected with U6-pshPHD2-A was higher than that from cells transfected with U6-pshPHD2-B. Moreover, the silencing effect of U6-pshPHD2-A on PHD2 as well as the increased level of VEGF secretion persisted for at least 18 days (**Figure 4b** and **c**).

PHD2 silencing promotes proliferation of HUVECs

We next investigated whether PHD2 silencing could increase endothelial cell proliferation. For this purpose, we first investigated the effect of PHD2 silencing on NIH3T3 cells. PHD2 silencing resulted in an increased proliferation of NIH3T3 cells (**Figure 5a**), probably because of the increase in the levels of growth factors, especially FGF2, which could also have the effect of enhancing the growth of fibroblast cells. We next determined the effect of the conditioned media from NIH3T3 cells on the proliferation of human umbilical vein endothelial cells (HUVECs). HUVECs treated with conditioned medium from PHD2-silenced cells showed significant increase in growth as compared to those treated with conditioned medium from controls (**Figure 5b**).

PHD2 silencing enhances angiogenesis *in vivo*

In order to test further whether PHD2 silencing is also effective in neoangiogenesis *in vivo*, we carried out the *in vivo* Matrigel plug assay as described earlier.[13] The results are shown in **Figure 6**. The areas shown in green represent the endothelium of vasculature, with the predominant linear structures indicating small vessels and some apparently circular structures indicating larger vessels. Structures double-positive for green (PECAM1) and red (SMA) (merged to yellow) indicate vessels with pericyte coverage, which are more mature vessels. Matrigel plugs mixed with NIH3T3 cells transfected with siPHD2-A exhibited slightly more neovascularization than those mixed with the cells transfected with control siRNA (**Figure 6a**). H and E staining also confirmed the results (**Figure 6a**, left). Next we investigated the effect of the U6-pshPHD2-A vector on neoangiogenesis. Matrigel plugs mixed with NIH3T3 cells transfected with U6-pshPHD2-A vector exhibited potent angiogenesis, with more pericyte-covered (and therefore more mature) neovasculature (**Figure 6b**), whereas Matrigel plugs mixed with cells transfected with control U6-pshRNA vector or mock cells exhibited almost no neoangiogenesis. The results of H and E staining also revealed that the U6-pshPHD2-A vector enhances neoangiogenesis, with tubelike structures containing red blood cells (arrowheads) exhibiting functional vasculature (**Figure 6b**, left). The quantification of mature neovasculature as revealed by the Matrigel plug assay, determined on the basis of pericyte-covered endothelium (vascular structures that are double-positive for SMA and PECAM), confirmed that PHD2 silencing, especially by the shPHD2 vector, enhances the induction of mature vasculature (**Figure 7**). The neoangiogenesis effect induced by the U6-pshPHD2-A vector resulted in an approximately fourfold increase in mature neovasculature, while the neoangiogenesis effect induced by the PHD2 siRNA resulted in only a twofold increase.

DISCUSSION

Therapeutic angiogenesis is a strategy involving the use of angiogenic molecules to induce the development of new blood vessels. However, because the clinical application of either recombinant VEGF or FGF2 by itself showed a less significant effect than expected,[8–10] the focus of therapeutic angiogenesis shifted to treatment using combinations of angiogenic molecules.[11–15] We have already confirmed that the combination treatment with recombinant VEGF and FGF2 has a synergistic effect on angiogenesis.[13] It follows, therefore, that a master regulator capable of simultaneously regulating multiple angiogenic growth factors might be a better choice for the target of gene therapy. An example of this kind of regulator is HIF-1, which plays an important role in angiogenesis by coordinately regulating the expression of multiple

Figure 1 Knockdown effect of prolyl hydroxylase domain-2 (PHD2)-suppressing small-interfering RNAs (siRNAs) and siRNA expression vectors on endogenous PHD2 mRNA expression and hypoxia inducible factor-1 (HIF-1) transcriptional activity. (**a**) The suppressive effect of PHD2-suppressing siRNAs on the endogenous PHD2 mRNA expression level in NIH3T3 cells. Cells were transfected with PHD2-suppressing siRNAs. Forty-eight and seventy-two hours after transfection, real-time reverse transcriptase-PCR (RT-PCR) analysis was performed. Nontargeting siRNA was used as control, and nontransfected cells at each time-point were also shown as mock. The data shown represent mean values ± SD, $n = 3$. (**b**) The effect of PHD2-suppressing U6-pshRNA expression vectors on endogenous PHD2 in NIH3T3 cells. Total RNA was collected from nontransfected cells and from cells transfected with the indicated U6-pshPHD2 expression vector or control U6 pshRNA expression vector, and real-time RT-PCR was performed. The results were normalized to the actin mRNA expression level, and shown relative to values from cells transfected with control vector. The data shown represent mean value ± SD, $n = 3$. (**c**) The effect of PHD2-suppressing CMV-pshRNA expression vectors on endogenous PHD2 in NIH3T3 cells. Real-time RT-PCR analysis was performed as described earlier. (**d–e**) The induction effect of PHD2 silencing on HIF-1 transcriptional activity in NIH3T3 cells. The cells were cotransfected with control vectors, or (**d**) the indicated U6 pshRNA expression vectors, or (**e**) CMV-pshRNA expression vectors, hypoxia-response reporter vector (5× hypoxia-responsive element promoter driven firefly luciferase reporter) and *Renilla* luciferase vector (pRL-SV40). Forty-eight hours later, dual luciferase assay was performed, and the results were normalized to the *Renilla* luciferase expression level. The data shown represent mean values ± SD, $n = 3$. (**f**) The suppressive effect of U6-pshPHD2-A expression vector on the endogenous PHD2 mRNA in NIH3T3 cells. The cells were transfected with U6-pshPHD2-A or control vector, selection was carried out, and real-time RT-PCR was performed to quantify PHD2 expression at the indicated time-points; nontransfected cells at each time-point were shown as mock. The results were normalized to the actin expression level and shown relative to the values from cells transfected with control vector. The data shown represent mean value ± SD, $n = 3$. shRNA, short-hairpin RNA.

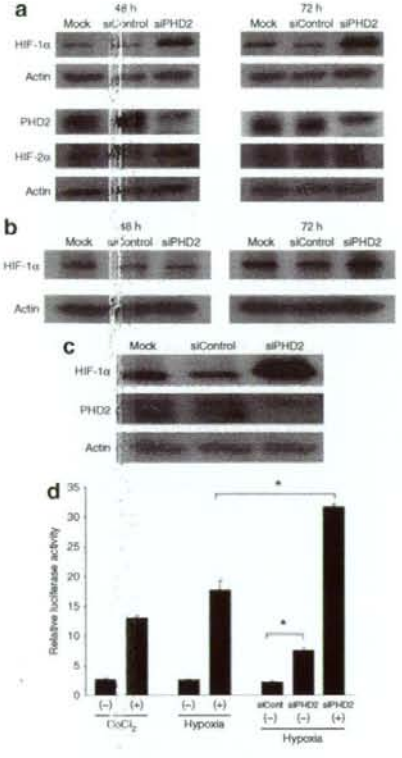

Figure 2 Prolyl hydroxylase domain-2 (PHD2) silencing induced stabilization of endogenous hypoxia-inducible factor-1α (HIF-1α) and increased HIF-1α transcriptional activity. (**a**) NIH3T3 cells were transfected with U6-pshPHD2-A or with control U6 vector, and Western blotting analysis was performed for detection of HIF-1α, HIF-2α, and PHD2 in the nuclei under normoxia conditions at the indicated time-points. Nontransfected cells were also shown as mock. Actin was used as a loading control. (**b**) Western blotting analysis of HIF-1α in the cytoplasm of cells transfected with U6 pshRNA expression vector and mock cells under normoxia conditions at the indicated time-points. (**c**) Western blotting analysis for detection of HIF-1α and PHD2 in the nuclei of cells transfected with U6 pshPHD2 expression vector or control vector, and mock cells under hypoxia conditions. NIH3T3 cells transfected with U6 pshRNA expression vectors were plated under hypoxia conditions (1% O_2) for 6 hours, and the nuclei extract of the cells was subjected to Western blotting analysis. (**d**) Effect of PHD2 silencing on the induction of HIF-1 transcriptional activity in cells exposed to $CoCl_2$ (a hypoxia-mimicking reagent), normoxia, or hypoxia conditions. NIH3T3 cells transfected with control siRNA vector or U6-pshpHD2-A vector were cotransfected with 5× hypoxia-responsive element promoter driven firefly luciferase reporter and *Renilla* luciferase vector, and then exposed to medium alone, medium containing $CoCl_2$ (100 μmol/l), or hypoxia conditions (1% O_2). Six hours later, dual luciferase assays were performed. The silencing of PHD2 significantly induced HIF-1 transcriptional activity under both normoxia (*$P < 0.05$) and hypoxia conditions (*$P < 0.05$), as compared to their respective controls. Results were normalized to the activity level of *Renilla* luciferase expression. The data shown represent mean value ± SD, $n = 3$. shRNA, short-hairpin RNA.

genes encoding critical angiogenic growth factors in a cell type–specific manner.[19] By virtue of its ability to upregulate multiple genes, HIF-1α has become an attractive molecular target for the treatment of ischemic or postischemic tissue injury.

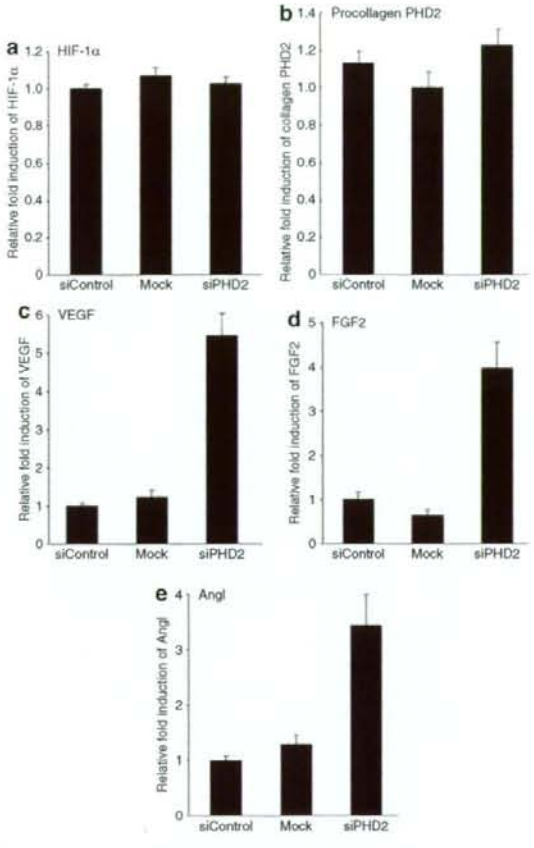

Figure 3 Effect of prolyl hydroxylase domain-2 (PHD2) silencing on angiogenic growth factor expression. NIH3T3 cells were transfected with U6-pshPHD2-A or with control vector, selection was carried out at 48 hours, and total RNA was isolated and subjected to real-time reverse transcriptase-PCR analysis: (**a**) hypoxia inducible factor-1α (HIF-1α); (**b**) procollagen PHD2; (**c**) vascular endothelial growth factor (VEGF); (**d**) fibroblast growth factor-2 (FGF2); and (**e**) angiopoietin-1 (Angl). Nontransfected cells were also shown as mock. The results were normalized to the mRNA expression level of actin and shown relative to cells transfected with control. The data shown represent mean value ± SD, $n = 3$.

Our results show that PHD2 silencing can functionally protect HIF-1α protein from proteasomal degradation and induce multiple angiogenic growth factors (VEGF, FGF2, and angiopoietin-1). However, to date, the *cis*-acting hypoxia-response elements (HIF-1 binding sites) have not been demonstrated in the regulatory regions of those angiogenic growth factor genes (except in VEGF). It remains to be determined, therefore, whether their regulation by HIF-1α is direct or indirect. Notably, we could not detect any obvious increase in the mRNA level of PDGF-B in NIH3T3 cells. This may be attributed to the fact that the regulation of angiogenic growth factors by HIF-1α is remarkably cell type–specific.[19] However, it is still possible that this silencing may induce the development of functional vessels. As shown in **Figure 3**, PHD2 silencing induced upregulation of both VEGF and FGF-2 in NIH3T3 cells. This result is consistent with the earlier report[13] showing that

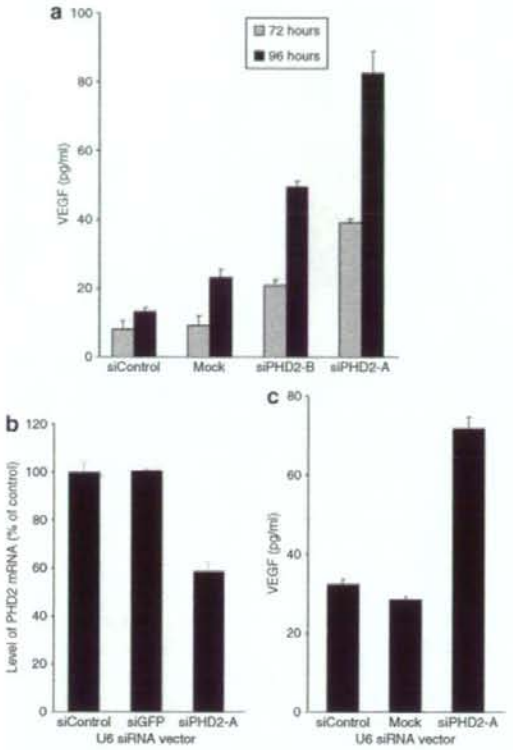

Figure 4 The induction effect of prolyl hydroxylase domain-2 (PHD2) silencing on the secretion of vascular endothelial growth factor (VEGF). NIH3T3 cells were transfected with U6-pshPHD2 vectors or with control vector for the indicated durations. (**a**) Quantification analysis of VEGF protein level in culture medium of cells transfected with U6-pshPHD2 vectors or control vector, and nontransfected cells (mock) by enzyme-linked immunosorbent assay (ELISA). (**b–c**) Long-term silencing effect of U6-pshPHD2-A in transfected cells 18 days after transfection: Real-time reverse transcriptase-PCR (RT-PCR) analysis was performed for the detection of PHD2 mRNA expression levels (**b**) and ELISA was performed for the detection of VEGF protein level in culture medium (**c**). The results of the real-time RT-PCR analysis were normalized to the mRNA expression level of actin, and shown relative to cells transfected with control vector. The data shown represent mean value ± SD, $n = 3$.

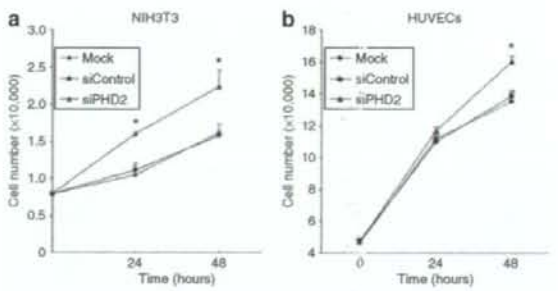

Figure 5 Prolyl hydroxylase domain-2 (PHD2) silencing promotes proliferation of NIH3T3 cells and human umbilical vein endothelial cells (HUVECs). (**a**) NIH3T3 cells transfected with U6-pshPHD2-A or with control vector were cultured further for the indicated durations, and cell numbers were counted. Nontransfected cells were also shown as mock. (**b**) HUVECs were cultured under serum-starved conditions, with conditioned medium obtained from U6-psh-PHD2-A- or control vector-transfected NIH3T3 cells or mock cells, and cell numbers were counted. Assays were performed in triplicate. The data shown represent mean value ± SD.

a combination of VEGF and FGF2 could synergistically induce more mature neovasculature through enhancement of endogenous PDGF-BB expression from endothelium, thereby gathering more pericytes to the endothelium through an enhanced gradient of PDGF-BB. Our results also showed that PHD2 silencing affects the proliferation of both NIH3T3 and HUVEC cells. This observation could be attributable to the increased expression of growth factors that induce signal-promoting cell proliferation. These results are consistent with published data showing that overexpression of PHD2 suppresses endothelial cell proliferation.[25]

In agreement with the earlier study,[28] our experiments showed that U6-pshPHD2 exhibited a stronger silencing effect than the CMV-pshPHD2 vector, thereby confirming that, at least at present, the U6 promoter (an RNA polymerase III promoter) is one of the most suitable promoters for expressing siRNAs, given its strong transcription activity[29] and absence of any extra sequence such as 5′-Cap and 3′-poly A.[28] We also confirmed that the pshPHD2 expression vector is more potent in inducing angiogenesis *in vivo* than the siRNA of the same target sequence. This might be because of the short half-life of siRNA, on account of degradation by intracellular RNase. Consequently, the continuous release of angiogenic growth factors for a long period, which is important for successful angiogenesis, could not be obtained. In general, therefore, two different approaches can be utilized for therapeutic applications: siRNA expression vectors for achieving middle- and long-term knockdown effect, and siRNAs for achieving short-term effect.

We have demonstrated, for the first time, that siRNA against PHD2 (HIF PHD2) can effectively induce neoangiogenesis by coordinately regulating the expression of multiple angiogenic growth factors through the stabilization of HIF-1α. Recently, Natarajan *et al.* showed that siRNA against procollagen prolyl 4-hydroxylase-2 (GenBank accession no. NM_011031, referred to also as "PHD2" mistakenly in their report, but in reality a different gene), can attenuate myocardial ischemia reperfusion injury and stabilize HIF-1α.[30] The phenotype they observed might be associated with the procollagen prolyl 4-hydroxylases-iNOS pathway, and not with the HIF prolyl hydroxylase/HIF/angiogenic growth factor pathway. Additionally, consistent with our results, Takeda *et al.*, using a conditional knockout mouse model, identified the role of HIF PHD2 in the adult vascular system.[31]

Earlier reports showed that, although the induction of angiogenesis using only VEGF does result in a vascular response, the induced vessel is unphysiologically permeable because of the absence of other external growth factors.[12] Direct expression of HIF-1α or HIF-1α lacking oxygen-sensitive degradation domain for angiogenesis has also been reported,[19,31] indicating that HIF-1α might be a good target for angiogenesis. However, the exogenous high and persistent expression of HIF1α[19] or oxygen-sensitive degradation domain–deficient HIF-1α[31] might result in some side effects such as development of cancers. Short-hairpin RNAs (shRNAs), expressed using nonviral vectors and synthetic siRNAs

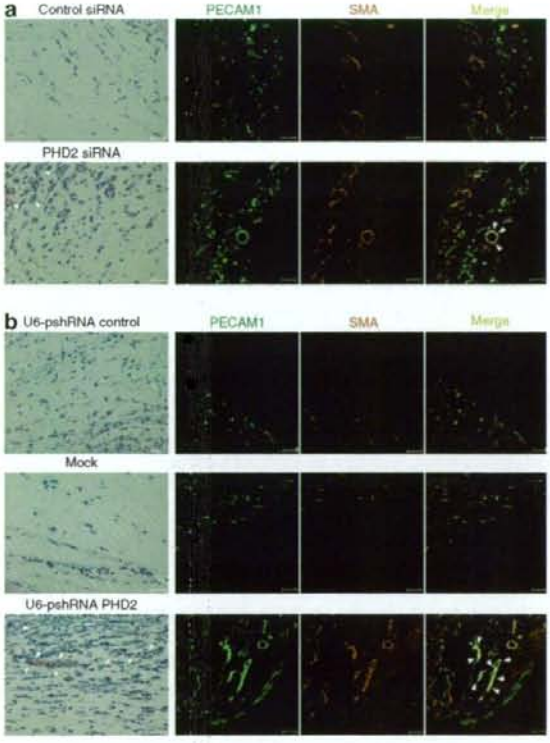

Figure 6 Prolyl hydroxylase domain-2 (PHD2) silencing enhances neoangiogenesis in a Matrigel plug assay *in vivo*. NIH3T3 cells transfected with (**a**) siPHD2-A, or (**b**) U6-psh-PHD2-A or their controls were mixed with Matrigel and injected subcutaneously into the abdominal region of 5-week-old female Balb/c mice ($n = 3$–5). After 7 days, the gels were excised and subjected to hematoxylin and eosin (H&E) staining (**a** and **b** left panels; scale bars = 40 μm), and to immunohistochemistry with anti-PECAM1 (shown in green, representing endothelium) and anti-SMA (shown in red, those adjacent to endothelium representing pericytes) (scale bars = 50 μm). Representative data from each experiment are shown. (**a**) Matrigel plug assay using cells transfected with siPHD2-A. siRNA-induced PHD2-silencing exhibited slightly more endothelium as compared to the control, with some of it covered by pericytes (arrow heads), (**a**: upper panels). (**b**) Matrigel plug assay using cells transfected with U6-psh-PHD2-A. U6-psh-PHD2-A vector-induced PHD2 silencing exhibited significantly more endothelium, with most of it covered by pericytes (arrowheads in immunohistochemistry) or more vessels containing red blood cells (arrowheads in H&E staining), as compared to the controls (**b**: upper panels) and to those mixed with cells transfected with siPHD2-A (**a**: lower panel). PECAM1, platelet-endothelial cell adhesion molecule-1; SMA, smooth muscle actin.

that are modified to enhance their stability, are potentially advantageous because of their temporary effect. PHD inhibitors have also been being explored as potential therapeutic agents; however, they are likely to lack adequate specificity. As shown in **Figure 3b** and **Supplementary Figure S4**, silencing of HIF-PHD2 has no influence on procollagen PHD2. Therefore, given its high specificity and strong effect, RNAi might be a better choice in therapeutic applications. Indeed, RNAi-based therapeutic applications have been in clinical trials for some diseases,[34,35] and some other preclinical trials are under development.[36–38]

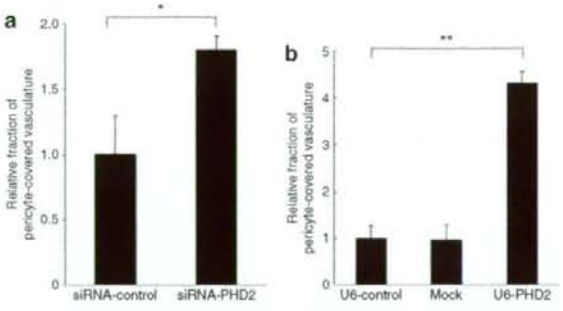

Figure 7 Quantification of the formation of new vessels in Matrigel plugs. (**a**) Quantification in Matrigel plug assay using cells transfected with siPHD2-A, and (**b**) quantification in Matrigel plug assay using cells transfected with U6-psh-PHD2-A. The quantification of the fraction of the pericyte-covered vasculature in whole neovasculature was performed by measuring the ratio of platelet-endothelial cell adhesion molecule-1 (PECAM1) to smooth muscle actin double-positive area (yellow area) within the PECAM1 area (green area), based on the immunohistochemistry results ($n = 9$). $^*P < 0.05$; $^{**}P < 0.01$. PHD2, prolyl hydroxylase domain-2; siRNA, small-interfering RNA.

In this study, we have demonstrated that implantation of PHD2-silenced cells is sufficient to enhance neoangiogenesis *in vivo*. These results could provide a basis for further therapeutic application, *i.e.*, using PHD2-suppressing RNAi as a potential strategy for angiogenic therapy. However, because of the limitation of our *in vivo* method, some further issues need to be addressed: (i) systematic evaluations on the basis of the functional aspects of regenerated vessels, including vascular hyperpermeability; (ii) additional preclinical and clinical studies, particularly in respect of safety and efficacy for therapeutic use in patients with ischemic cardiovascular diseases such as myocardial infarction; (iii) the development of delivery systems to deliver the siRNA expression vector and/or siRNA to the target sites and to make them functional in an efficient and safe manner. In this regard, we have explored polymeric micelle-based nanocarriers for plasmid DNA[39,40] and siRNA,[41,42] and demonstrated their *in vitro* and *in vivo* efficacies, including efficient gene transfer to primary cells,[40] *in vivo* transfection to a rabbit carotid artery,[43] and transfection-mediated bone regeneration.[44] We intend to further investigate the use of these nanocarriers in PHD2-silencing-mediated neoangiogenesis therapy.

MATERIALS AND METHODS

Cell lines and culture. The mouse fibroblast cells NIH3T3 (Riken Cell Bank, Tsukuba, Japan) were cultured in Dulbecco's modified Eagle's medium (Sigma-Aldrich, St. Louis, MO) containing 10% fetal bovine serum (Sigma-Aldrich). HUVECs (Lonza, Walkersville, MD) were maintained in the angiogenic medium EBM2 plus EGM2 (Lonza).

Preparation of siRNA expression vectors. siRNAs of murine PHD2 and PHD3 (GenBank accession no. NM_053207 and NM_028133, respectively) were synthesized (Dharmacon, Lafayette, Colorado). The sense sequences of DNA corresponding to murine PHD2-duplex siRNAs were 5′-GAACTCAAGCCCAATTCAG-3′ (siPHD2-A) and 5′-TGAG CGAGCGAGAGCTAAA-3′ (siPHD2-B). The sense sequence of DNA corresponding to murine PHD3-duplex siRNAs was 5′-GGCAAT GGTGGCTTGCTAT-3′. The SMART pool siRNAs of murine PHD2 and nontargeting siRNA containing 21 nucleotide sequences with no homology

to murine genes, which was used for control (NTSC), were also purchased from Dharmacon. Luciferase reporter gene assays were carried out using plasmid DNA encoding luciferase driven by the 5× hypoxia-responsive element (5×HRE) promoter, kindly supplied by Dr. Kondo of the Graduate School of Medicine, Kyoto University. The shRNA expression vectors were constructed by placing oligonucleotides based on the two siRNAs of murine PHD2 and PHD3 (mentioned earlier) into pSilencer 2.1-U6 or pSilencer 4.1-CMV (nos. 5762 and 5775, respectively; Ambion, Austin, TX) in accordance with the manufacturer's instructions.

Transient transfections and dual luciferase reporter assays. NIH3T3 cells were seeded in 24-well dishes at 1.5×10^5 cells/dish. The next day, the cells were cotransfected with the indicated siRNA expression vectors, 5×HRE reporter and *Renilla* luciferase expression vector (pRL-SV40, Promega), using FuGENE6 reagent (Roche Applied Science, Mannheim, Germany). Twenty-four hours after cotransfection, the cells were exposed to either medium alone, or medium containing $CoCl_2$ (100 μmol/l), and then incubated for 6 hours so as to chemically stabilize HIF-1α. For the hypoxia-environment experiment, 24 hours after cotransfection the siRNA vector-transfected NIH3T3 cells were plated into an Anaeropouch Box (1% O_2; Mitsubishi GAS chemical Company, Tokyo, Japan) and cultured for 6 hours. Dual luciferase assays were then performed using the Dual Luciferase Assay System (Promega). Relative luciferase activities were determined by calculating the ratio between the activity levels of firefly and *Renilla* luciferase. The results are shown as mean value ± SD ($n = 3$). For siRNA experiments, NIH3T3 cells were first transfected with the indicated siRNA for 12 hours using Lipofectamine 2000 (Invitrogen, Carlsbad, CA), and then cotransfected with 5×HRE reporter and *Renilla* luciferase expression vectors. Dual luciferase assays were performed 24 hours later.

Quantitative RT-PCR analysis. RNA was purified using TRIZOL reagent and the RNeasy column (Invitrogen). Total RNA (1 μg) treated with DNase I (Qiagen, Hilden, Germany) was reverse transcribed using QuantiTect Reverse Transcription (Qiagen), and real-time RT-PCR was performed using the ABI 7500 Fast Real-time RT-PCR System (Applied Biosystems, Foster City, CA) and QuantiTect SYBR Green PCR Master Mix (Qiagen). All reactions were run in triplicate. All expression data were normalized to actin. The sequences of the primers used are listed in **Supplementary Table S1**.

Western blot analysis. Whole cells were collected by centrifugation. The separation of nuclear and cytoplasmic extract was performed using an NE-PER Kit (Pierce, Rockford, IL). Sample proteins were electrophoresed on sodium dodecyl sulfate polyacrylamide gel electrophoresis and transferred to a polyvinylidene fluoride membrane (Bio-Rad, Hercules, CA). Western blottings were performed as described earlier.[45] Primary antibodies against mouse HIF-1α (NB100-449; Novus Biological, Littleton, CO), HIF-2α (NB100-122; Novus), PHD2 (NB100-2219; Novus), and actin (Sigma-Aldrich) were used for detecting the corresponding protein.

Enzyme-linked immunosorbent assay. NIH3T3 cells were transfected with the indicated siRNAs or siRNA expression vectors. For siRNA vector-transfected cells, a selection was carried out 24 hours after transfection so as to eliminate the untransfected cells. The transfected cells were seeded onto 24-well plates. Culture supernatants were harvested at the indicated time-points. VEGF was measured using a commercially available sandwich immunoassay kits (MMV00; R&D Systems, Minneapolis, MN).

Cell viability assays. HUVECs were seeded into collagen I–coated 24-well culture plates at a density of 3×10^4 cells/well. After 24 hours, the medium was changed to Dulbecco's modified Eagle's medium containing 1% fetal bovine serum and 20% conditioned medium, and plates were again incubated at 37°C in 5% CO_2. The viable cells were counted 24 and 48 hours after additional culture, using colorimetric assays with 2-(2-methoxy-4-nitrophenyl)-3-(4-nitrophenyl)-5-(2,4-disulphophenyl)-2H-tetrazolioum monosodium salt (Cell Counting Kit-8; Dojindo, Kumamoto, Japan) in accordance with the manufacture's instructions. For cell viability assays in NIH3T3 cells, the cells transfected by the siRNA control expression vector and those transfected by the siPHD2 expression vector were seeded into 48-well culture plates at a density of 8,000 cells/well in Dulbecco's modified Eagle's medium. After 24 and 48 hours, live cells were counted as described earlier.

In vivo *Matrigel plug assay.* NIH3T3 cells were transfected with siRNA expression vector of murine PHD2 (pSilencer 2.1-U6 puro) using FuGENE6 (Roche Applied Science). After 24 hours, selection was performed with puromycin so as to eliminate untransfected cells. Two days later, the selected cells were harvested. 1.0×10^6 NIH3T3 cells were mixed with regular Matrigel (BD Biosciences, Bedford, MA). The Matrigels (400 μl each) were injected subcutaneously into the abdominal region of female Balb/c mice (CLEA Japan, Tokyo, Japan). Each mouse was injected with one implant. Each experiment performed on three to five mice. The Matrigel plugs were removed on day 7, and were either directly frozen in dry-iced acetone for immunohitochemistry or fixed with formalin and paraffin-embedded for H&E staining. For the Matrigel plug assay mixed with siRNA-transfected cells, NIH3T3 cells were mixed with Matrigel and injected into the mice 24 hours after transfection with control siRNA and PHD2 siRNA. All experiment protocols were conducted in accordance with the policies of the Animal Ethics Committee at the University of Tokyo.

Immunohistochemistry of Matrigel plugs. The frozen matrigel plugs were sliced into sections of 10 μm thickness using a cryostat. The fixed sections were incubated with antimurine PECAM1 (Clone Mec13.3; BD Pharmingen 553730, BD Biosciences Pharmingen, San Diego, CA) for 1 hour. The specimens were subsequently stained with antirat/IgG conjugated with Alexa Fluor 488 (Invitrogen Molecular Probes) and monoclonal antimurine α-SMA Cy3 conjugate (Sigma-Aldrich) for 1 hour at room temperature. Confocal laser scanning analysis was performed using an LSM 510 microscope (Carl Zeiss, Germany) at an excitation wavelength of 488 and 543 nm.

Quantification in Matrigel plug assays. We quantified the formation of mature vessel structures in Matrigel plugs by measuring the ratio of the PECAM1 area to the SMA-postive (yellow) area within the PECAM1-postive (green) area using LSM image software (Carl Zeiss), yielding the fraction of endothelial-positive structures that are co-positive for smooth muscle structures. Microsoft Excel software was used for statistical analysis. The data represent average values from nine areas from three independent Matrigel plugs.

ACKNOWLEDGMENTS

This work was supported by the Core Research Program for Evolutional Science and Technology from the Japan Science and Technology Agency, and Grants-in-Aid for Scientific Research from the Japanese Ministry of Education, Culture, Sports, Science and Technology. The authors declare that they have no conflict of interest.

SUPPLEMENTARY MATERIAL

Figure S1. PHD2-silencing via siRNAs induced HIF-1 transcriptional activity in NIH3T3 cells and C2C12 cells.
Figure S2. PHD2-silencing via siRNAs induced VEGF mRNA expression in NIH3T3 cells.
Figure S3. PHD2-silencing via siRNAs induced the secretion of VEGF.
Figure S4. The influence of PHD2-silencing induced siRNA on procollagen PHD2.
Table S1. Primers used for real-time RT-PCR.

REFERENCES

1. Olsson, AK, Dimberg, A, Kreuger, J and Claesson-Welsh, L (2006). VEGF receptor signalling - in control of vascular function. *Nat Rev Mol Cell Biol* **7**: 359–371.

2. Shibuya, M and Claesson-Welsh, L (2006). Signal transduction by VEGF receptors in regulation of angiogenesis and lymphangiogenesis. *Exp Cell Res* **312**: 549–560.
3. Magnusson, P, Rolny, C, Jakobsson, L, Wikner, C, Wu, Y, Hicklin, DJ *et al.* (2004). Deregulation of Flk-1/vascular endothelial growth factor receptor-2 in fibroblast growth factor receptor-1-deficient vascular stem cell development. *J Cell Sci* **117**: 1513–1523.
4. Carmeliet, P, Ferreira, V, Breier, G, Pollefeyt, S, Kieckens, L, Gertsenstein, M *et al.* (1996). Abnormal blood vessel development and lethality in embryos lacking a single VEGF allele. *Nature* **380**: 435–439.
5. Detmar, M, Brown, LF, Schon, MP, Elicker, BM, Velasco, P, Richard, L *et al.* (1998). Increased microvascular density and enhanced leukocyte rolling and adhesion in the skin of VEGF transgenic mice. *J Invest Dermatol* **111**: 1–6.
6. Bikfalvi, A, Klein, S, Pintucci, G and Rifkin, DB (1997). Biological roles of fibroblast growth factor-2. *Endocr Rev* **18**: 26–45.
7. Lee, SH, Schloss, DJ and Swain, JL (2000). Maintenance of vascular integrity in the embryo requires signaling through the fibroblast growth factor receptor. *J Biol Chem* **275**: 33679–33687.
8. Simons, M, Annex, BH, Laham, RJ, Kleiman, N, Henry, T, Dauerman, H *et al.* (2002). Pharmacological treatment of coronary artery disease with recombinant fibroblast growth factor-2: double-blind, randomized, controlled clinical trial. *Circulation* **105**: 788–793.
9. Henry, TD, Annex, BH, McKendall, GR, Azrin, MA, Lopez, JJ, Giordano, FJ *et al.* (2003). The VIVA trial: Vascular endothelial growth factor in Ischemia for Vascular Angiogenesis. *Circulation* **107**: 1359–1365.
10. Lederman, RJ, Mendelsohn, FO, Anderson, RD, Saucedo, JF, Tenaglia, AN, Hermiller, JB *et al.* (2002). Therapeutic angiogenesis with recombinant fibroblast growth factor-2 for intermittent claudication (the TRAFFIC study): a randomised trial. *Lancet* **359**: 2053–2058.
11. Pepper, MS, Ferrara, N, Orci, L and Montesano, R (1992). Potent synergism between vascular endothelial growth factor and basic fibroblast growth factor in the induction of angiogenesis *in vitro*. *Biochem Biophys Res Commun* **189**: 824–831.
12. Asahara, T, Bauters, C, Zheng, LP, Takeshita, S, Bunting, S, Ferrara, N *et al.* (1995). Synergistic effect of vascular endothelial growth factor and basic fibroblast growth factor on angiogenesis *in vivo*. *Circulation* **92**: II365–II371.
13. Kano, MR, Morishita, Y, Iwata, C, Iwasaka, S, Watabe, T, Ouchi, Y *et al.* (2005). VEGF-A and FGF-2 synergistically promote neoangiogenesis through enhancement of endogenous PDGF-B-PDGFRbeta signaling. *J Cell Sci* **118**: 3759–3768.
14. Richardson, TP, Peters, MC, Ennett, AB and Mooney, DJ (2001). Polymeric system for dual growth factor delivery. *Nat Biotechnol* **19**: 1029–1034.
15. Cao, R, Brakenhielm, E, Pawliuk, R, Wariaro, D, Post, MJ, Wahlberg, E *et al.* (2003). Angiogenic synergism, vascular stability and improvement of hind-limb ischemia by a combination of PDGF-BB and FGF-2. *Nat Med* **9**: 604–613.
16. Appelhoff, RJ, Tian, YM, Raval, RR, Turley, H, Harris, AL, Pugh, CW *et al.* (2004). Differential function of the prolyl hydroxylases PHD1, PHD2, and PHD3 in the regulation of hypoxia-inducible factor. *J Biol Chem* **279**: 38458–38465.
17. Semenza, GL (2003). Targeting HIF-1 for cancer therapy. *Nat Rev Cancer* **3**: 721–732.
18. Elson, DA, Thurston, G, Huang, LE, Ginzinger, DG, McDonald, DM, Johnson, RS *et al.* (2001). Induction of hypervascularity without leakage or inflammation in transgenic mice overexpressing hypoxia-inducible factor-1α. *Genes Dev* **15**: 2520–2532.
19. Kelly, BD, Hackett, SF, Hirota, K, Oshima, Y, Cai, Z, Berg-Dixon, S *et al.* (2003). Cell type-specific regulation of angiogenic growth factor gene expression and induction of angiogenesis in nonischemic tissue by a constitutively active form of hypoxia-inducible factor 1. *Circ Res* **93**: 1074–1081.
20. Fire, A, Xu, S, Montgomery, MK, Kostas, SA, Driver, SE and Mello, CC (1998). Potent and specific genetic interference by double-stranded RNA in *Caenorhabditis elegans*. *Nature* **391**: 806–811.
21. Hannon, GJ and Rossi, JJ (2004). Unlocking the potential of the human genome with RNA interference. *Nature* **431**: 371–378.
22. Paddison, PJ, Silva, JM, Conklin, DS, Schlabach, M, Li, M, Aruleba, S *et al.* (2004). A resource for large-scale RNA-interference-based screens in mammals. *Nature* **428**: 427–431.
23. Leung, RK and Whittaker, PA (2005). RNA interference: from gene silencing to gene-specific therapeutics. *Pharmacol Ther* **107**: 222–239.
24. Behlke, MA (2006). Progress towards *in vivo* use of siRNAs. *Mol Ther* **13**: 644–670.
25. Takeda, K and Fong, GH (2007). Prolyl hydroxylase domain 2 protein suppresses hypoxia-induced endothelial cell proliferation. *Hypertension* **49**: 178–184.
26. Busca, R, Berra, E, Gaggioli, C, Khaled, M, Bille, K, Marchetti, B *et al.* (2005). Hypoxia-inducible factor 1α is a new target of microphthalmia-associated transcription factor (MITF) in melanoma cells. *J Cell Biol* **170**: 49–59.
27. Berra, E, Benizri, E, Ginouves, A, Volmat, V, Roux, D and Pouyssegur, J (2003). HIF prolyl-hydroxylase 2 is the key oxygen sensor setting low steady-state levels of HIF-1α in normoxia. *EMBO J* **22**: 4082–4090.
28. Makinen, PI, Koponen, JK, Karkkainen, AM, Malm, TM, Pulkkinen, KH, Koistinaho, J *et al.* (2006). Stable RNA interference: comparison of U6 and H1 promoters in endothelial cells and in mouse brain. *J Gene Med* **8**: 433–441.
29. Weinberg, RA and Penman, S (1968). Small molecular weight monodisperse nuclear RNA. *J Mol Biol* **38**: 289–304.
30. Natarajan, R, Salloum, FN, Fisher, BJ, Kukreja, RC and Fowler, AA 3rd (2006). Hypoxia inducible factor-1 activation by prolyl 4-hydroxylase-2 gene silencing attenuates myocardial ischemia reperfusion injury. *Circ Res* **98**: 133–140.
31. Takeda, K, Cowan, A and Fong, GH (2007). Essential role for prolyl hydroxylase domain protein 2 in oxygen homeostasis of the adult vascular system. *Circulation* **116**: 774–781.
32. Lee, RJ, Springer, ML, Blanco-Bose, WE, Shaw, R, Ursell, PC and Blau, HM (2000). VEGF gene delivery to myocardium: deleterious effects of unregulated expression. *Circulation* **102**: 898–901.
33. Trentin, D, Hall, H, Wechsler, S and Hubbell, JA (2006). Peptide-matrix-mediated gene transfer of an oxygen-insensitive hypoxia-inducible factor-1α variant for local induction of angiogenesis. *Proc Natl Acad Sci USA* **103**: 2506–2511.
34. Check, E (2005). A crucial test. *Nat Med* **11**: 243–244.
35. Bitko, V, Musiyenko, A, Shulyayeva, O and Barik, S (2005). Inhibition of respiratory viruses by nasally administered siRNA. *Nat Med* **11**: 50–55.
36. Kim, DH and Rossi, JJ (2007). Strategies for silencing human disease using RNA interference. *Nat Rev Genet* **8**: 173–184.
37. Dykxhoorn, DM and Lieberman, J (2006). Silencing viral infection. *PLoS Med* **3**: e242.
38. Raoul, C, Barker, SD and Aebischer, P (2006). Viral-based modelling and correction of neurodegenerative diseases by RNA interference. *Gene Ther* **13**: 487–495.
39. Miyata, K, Kakizawa, Y, Nishiyama, N, Harada, A, Yamasaki, Y, Koyama, H *et al.* (2004). Block catiomer polyplexes with regulated densities of charge and disulfide cross-linking directed to enhance gene expression. *J Am Chem Soc* **126**: 2355–2361.
40. Kanayama, N, Fukushima, S, Nishiyama, N, Itaka, K, Jang, WD, Miyata, K *et al.* (2006). A PEG-based biocompatible block catiomer with high buffering capacity for the construction of polyplex micelles showing efficient gene transfer toward primary cells. *ChemMedChem* **1**: 439–444.
41. Oishi, M, Nagasaki, Y, Itaka, K, Nishiyama, N and Kataoka, K (2005). Lactosylated poly(ethylene glycol)-siRNA conjugate through acid-labile β-thiopropionate linkage to construct pH-sensitive polyion complex micelles achieving enhanced gene silencing in hepatoma cells. *J Am Chem Soc* **127**: 1624–1625.
42. Kakizawa, Y, Furukawa, S, Ishii, A and Kataoka, K (2006). Organic-inorganic hybrid-nanocarrier of siRNA constructing through the self-assembly of calcium phosphate and PEG-based block aniomer. *J Control Release* **111**: 368–370.
43. Akagi, D, Oba, M, Koyama, H, Nishiyama, N, Fukushima, S, Miyata, T *et al.* (2007). Biocompatible micellar nanovectors achieve efficient gene transfer to vascular lesions without cytotoxicity and thrombus formation. *Gene Ther* **14**: 1029–1038.
44. Itaka, K, Ohba, S, Miyata, K, Kawaguchi, H, Nakamura, K, Takato, T *et al.* (2007). Bone regeneration by regulated *in vivo* gene transfer using biocompatible polyplex nanomicelles. *Mol Ther* **15**: 1655–1662.
45. Wu, S, Murai, S, Kataoka, K and Miyagishi, M (2008). Yin Yang 1 induces transcriptional activity of p73 through cooperation with E2F1. *Biochem Biophys Res Commun* **365**: 75–81.

Cell Transfection

DOI: 10.1002/anie.200800963

Charge-Conversion Ternary Polyplex with Endosome Disruption Moiety: A Technique for Efficient and Safe Gene Delivery**

*Yan Lee, Kanjiro Miyata, Makoto Oba, Takehiko Ishii, Shigeto Fukushima, Muri Han, Hiroyuki Koyama, Nobuhiro Nishiyama, and Kazunori Kataoka**

DNA or RNA delivery into target cells by synthetic nonviral vectors (lipoplexes and polyplexes) is widely recognized as a promising alternative to delivery with viral vectors, which encounter the safety issues inherent to their biological propensities.[1] Nevertheless, even in the case of nonviral vectors, the inconsistency between the delivery efficiency and the safety issue, particularly with regard to chemotoxicity, has been a major matter of concern. The vectors with high transfection efficiency often show high toxicity, whereas those with low toxicity frequently raise the issue of low transfection efficiency.

Various polycations with regulated basicity have been developed for the construction of polyplexes directed toward high transfection efficiency since Behr and co-workers introduced to the gene-delivery field the concept of endosomal escape through the "proton-sponge" effect hypothesized for polyethyleneimine (PEI), yet the toxicity of these polycations lends the polyplexes to only limited applications.[2] One of the main reasons for the limited success is probably that different, and even conflicting, functionalities of the polyplexes are required at each different stage of the delivery processes. For example, the moieties of high amine density in the polyplexes are important to overcome endosomal membrane barriers because their protonation potential contributes to endosome buffering as well as to membrane destabilization.[3] On the other hand, the positively charged nature of the polyplexes may induce nonspecific interactions with negatively charged serum components to form thrombi in the capillary and carries the risk of perturbing the structure of the plasma membrane to induce high cytotoxicity and excessive immune responses.[4] Shielding of the positive charges by covering the polyplex surface with polyanions[5] or poly(ethylene glycol) (PEG)[6] is a well-known practical solution to these problems, yet significant lowering of the transfection efficiency is inevitable, mainly due to the reduced cellular uptake and the impaired capacity for endosome escape. Therefore, much effort has been concentrated on the development of deshielding methods at a specific stage during the transfection process.[7]

Herein, we wish to communicate a novel approach to the design of polyplexes exerting both high transfection efficiency and lowered cytotoxicity by integrating a charge-conversion moiety into the polyplex structure. Maleic amide derivatives, *cis*-aconitic amide, and citraconic amide have negative charges at neutral pH values, but they degrade promptly at weakly acidic pH 5.5 to expose positively charged amines.[8] Therefore, if we cover the surface of the positively charged polyplexes with degradable amide-derivatized polymers to form ternary polyplexes (plasmid DNA/polycation/polyanion with the degradable side chain), the polyplexes maintain a neutral to negatively charged nature on the cell exterior, whereas the charge-conversion components are expected to turn positive in the acidic milieu of the endosome to facilitate the endosomal escape of the polyplexes through membrane disruption (Figure 1).

Initially, a polyplex between plasmid DNA (pDNA) and a polycation was prepared. As the polycation, we chose pAsp-(DET) (Figure 2A), which had been proven by our group to be an endosome-disrupting and membrane-destabilization moiety with lower cytotoxicity than conventional polycations, including PEI.[9] The polyplexes showed positive surface charges with a zeta potential of approximately +40 mV because of the excess amount of polycations (N (amines in pAsp(DET))/P (phosphate in pDNA) ratio of 4–8). The polyplex was then added to 1–4 molar equivalents of the charge-conversion polymer pAsp(DET-Aco) (Figure 2A) to form the ternary polyplex. The pAsp(DET-Aco) should turn into pAsp(DET), which could also disrupt the endosome efficiently, at the endosomal pH value after degradation of the *cis*-aconitic amide moieties. Each ternary polyplex at various charge ratios showed unimodal size distribution with a mean diameter of about 130 nm, as measured by dynamic light scattering (DLS), even in the presence of excess pAsp(DET-Aco). Although there is a possibility of the formation of the binary polyplex between pAsp(DET-Aco)

[*] Dr. Y. Lee, S. Fukushima, Dr. N. Nishiyama, Prof. Dr. K. Kataoka
Division of Clinical Biotechnology, Center for Disease Biology and Integrative Medicine, Graduate School of Medicine, University of Tokyo, 7-3-1 Hongo, Bunkyo-ku, Tokyo 113-0033 (Japan)
Fax: (+81) 3-5841-7139
E-mail: kataoka@bmw.t.u-tokyo.ac.jp
Dr. K. Miyata, Dr. T. Ishii, Prof. Dr. K. Kataoka
Department of Bioengineering, University of Tokyo
7-3-1 Hongo, Bunkyo-ku, Tokyo 113-0033 (Japan)
Dr. M. Oba, Prof. Dr. H. Koyama
Department of Clinical Vascular Regeneration, University of Tokyo
7-3-1 Hongo, Bunkyo-ku, Tokyo 113-0033 (Japan)
Dr. K. Miyata, Dr. N. Nishiyama, Prof. Dr. K. Kataoka
Center for Nanobio Integration, University of Tokyo
7-3-1 Hongo, Bunkyo-ku, Tokyo 113-8656 (Japan)
Dr. M. Han, Prof. Dr. K. Kataoka
Department of Materials Engineering, University of Tokyo
7-3-1 Hongo, Bunkyo-ku, Tokyo 113-8656 (Japan)

[**] This work was supported by a Core Research for Evolutional Science and Technology (CREST) grant from the Japan Science and Technology Agency (JST).

Supporting information for this article is available on the WWW under http://www.angewandte.org or from the author.

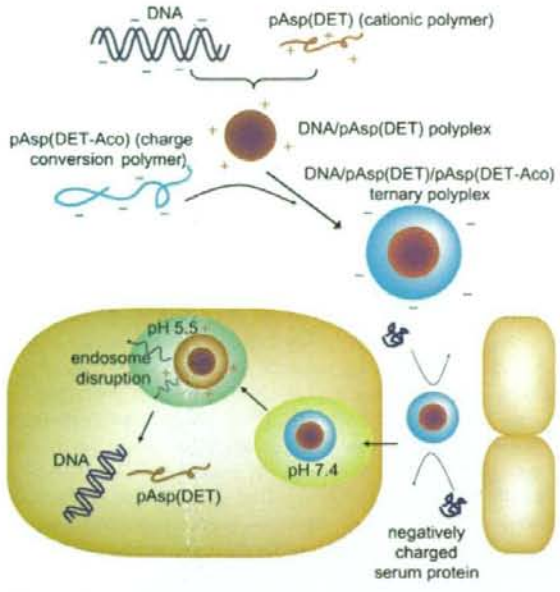

Figure 1. Diagram of the charge-conversion ternary polyplex with an endosome-disrupting function. pAsp(DET): poly{*N*-[*N*'-(2-aminoethyl)-2-aminoethyl]aspartamide}; pAsp(DET-Aco): poly(*N*-{*N*'-[(*N*''-*cis*-aconityl)-2-aminoethyl]-2-aminoethyl}aspartamide).

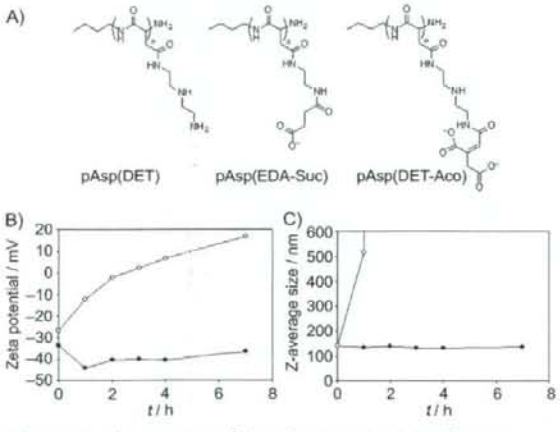

Figure 2. A) The structures of the polycation pAsp(DET), the non-charge-conversion polyanion poly[(*N*'-succinyl-2-aminoethyl)aspartamide] (pAsp(EDA-Suc)), and the charge-conversion polyanion pAsp(DET-Aco). B) The charge conversion of the ternary polyplex of DNA/pAsp(DET)/pAsp(DET-Aco). C) The change of hydrodynamic diameter of the ternary polyplex. ○: results at pH 5.5; ●: results at pH 7.4.

and pAsp(DET) without DNA, the formation of the DNA-containing ternary polyplex was confirmed by gel electrophoresis assays (see the Supporting Information).

The charge-conversion behavior of the ternary polyplex was monitored from the change in the zeta potential, as illustrated in Figure 2B. The ternary polyplex maintained a zeta potential of around −40 mV at pH 7.4. However, the zeta potential at pH 5.5 increased gradually from negative to positive; this result indicates the charge conversion due to the degradation of the *cis*-aconitic amide moieties. After incubation for 2 h at pH 5.5, the zeta potential reached 0 mV. As a negative control, we used a non-charge-conversion polyanion with a similar structure, pAsp(EDA-Suc) (Figure 2A). The ternary polyplex with pAsp(DET) and pAsp(EDA-Suc) maintained a zeta potential of around −40 mV at pH 5.5 and pH 7.4, and it showed no sign of charge conversion (see the Supporting Information).

The charge conversion also induced a dramatic size change in the ternary polyplex. As shown in Figure 2C, the ternary polyplex maintained a diameter of around 130 nm at pH 7.4, but there was an immediate increase in its size at pH 5.5, even after 1 h. After 2 h, large aggregates with a diameter of over 1 μm had formed. The reason for the aggregation is probably the reduction in the repulsive forces due to the partial charge neutralization after 1 h and the complete neutralization after 2 h at pH 5.5, as indicated from the data of the zeta potential measurements.

For the potential in vivo applications, the polyplex stability in a solution of serum proteins should be addressed. In a solution of bovine serum albumin (BSA), the ternary polyplexes maintained their original diameter, whereas the positive polyplex of pAsp(DET) showed a prompt increase in diameter, even after 1 h of incubation (Figure 3A). The improved stability of the ternary polyplex was probably due to the repulsive forces between the anionic ternary polyplex and the BSA; this could be a merit for future systemic applications.

The transfection was performed by using human umbilical vein endothelial cells (HUVEC). Only limited transfection reagents have been available for these cells in the past because they are very difficult to transfect and sensitive to toxicity.[10]

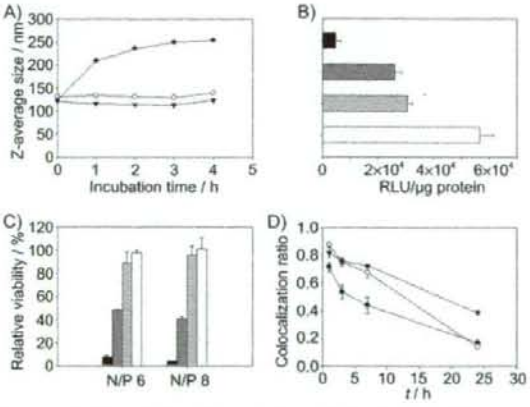

Figure 3. A) The stability of the polyplex in BSA solution. B) The transfection activity of the various vectors. C) The relative viability of HUVEC transfected with the various vectors. D) The colocalization ratio of the red fluorescence of cyanine-5-labeled DNA with the green fluorescence of LysoTracker Green (see Figure 4). Error bars indicate the standard error. Black bars: ExGen 500; ● and dark gray bars: pAsp(DET) polyplex; ▼ and light gray bars: pAsp(EDA-Suc) ternary polyplex; ○ and white bars: pAsp(DET-Aco) ternary polyplex.

The resulting transfection data with luciferase pDNA are summarized in Figure 3B. The N/P ratios between DNA and pAsp(DET) in both the simple polyplex and the ternary polyplex were 6, the value at which they showed the highest transfection efficiency. The ternary polyplexes were formed by addition of two molar equivalents of pAsp(DET-Aco) or pAsp(EDA-Suc) to the simple polyplex. The control ternary polyplex with pAsp(EDA-Suc) showed similar transfection efficiency to the simple polyplex of pAsp(DET), whereas the charge-conversion ternary polyplex of pAsp(DET-Aco) showed a tranfection efficiency that was more than ten times higher than that of ExGen 500, a commercially available transfection reagent of linear PEI, and two times higher than that of the pAsp(DET) polyplex. Even though the negative surface charge of the ternary complex was not helpful for the cellular uptake and endosomal escape, it increased the stability of the complex in the presence of the serum proteins, as shown in Figure 3A, and reduced the toxicity, so that the non-charge-conversion ternary polyplex (DNA/pAsp(DET)/pAsp(DET-Suc)) showed similar transfection efficiency to the simple polyplex. With the introduction of the charge-conversion endosome-disrupting moiety into the ternary polyplex on the basis of that stability and low toxicity (DNA/pAsp(DET)/pAsp(DET-Aco)), the transfection efficiency was still more increased. The transfection results with yellow-fluorescence-protein (YFP) pDNA, which also showed the appreciable transfection efficiency of the ternary polyplex system, is summarized in the Supporting Information.

The cytotoxicity, as measured by an MTT viability assay, is shown in Figure 3C. At N/P ratios of 6 and 8, which were the optimal ratios for the transfection, ExGen 500 showed very high toxicity with a viability below 10%, and the pAsp(DET) polyplex also showed the viability to be decreased to 50%. One of the main reasons for the decreased viability was probably the positive surface charge of the polyplexes inducing membrane toxicity.[11] However, the ternary polyplexes, which had negatively charged surfaces at the cell exterior, showed almost no cytotoxicity at both N/P ratios.

For the confirmation of the enhanced endosomal escape of the charge-conversion ternary polyplex, the intracellular distribution of the polyplex was investigated by confocal laser scanning microscopy (CLSM) by using cyanine-5-labeled pDNA (Figure 4). The yellow fluorescence changes to red when the polyplex is released from the acidic vasicular organelles. The positively charged pAsp(DET) polyplex showed significant endosomal escape, even only after 3 h, and over 80% of the DNA had escaped after 24 h. Both ternary polyplexes showed low endosomal escape after 3 h. However, the charge-conversion ternary polyplex from pAsp(DET-Aco) showed similar levels of endosomal escape to the positive pAsp(DET) polyplex after 24 h, whereas large portions (over 40%) of the non-charge-conversion ternary polyplex with pAsp(EDA-Suc) still remained in the endosomes.

The quantitative analyses of the CLSM images are summarized in Figure 3D. The charge-conversion polyplex showed similar behavior to the non-charge-conversion polyplex until 3 h, but it showed less colocalization ratio after 7 h, and finally had a similar ratio to the positive pAsp(DET) polyplex after 24 h. By considering that the endosomal acidification and the charge conversion required some time, the CLSM data were reasonable and agreed with the luciferase transfection data.

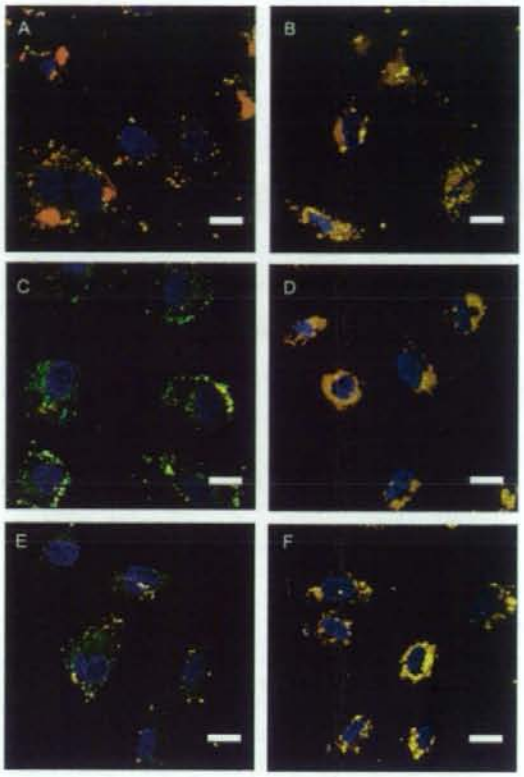

Figure 4. CLSM images of HUVEC transfected with pAsp(DET) polyplex (A and B), pAsp(DET-Aco) ternary polyplex (C and D), and pAsp(EDA-Suc) ternary polyplex (E and F). (A, C, and E) are images after 3 h of transfection; (B, D, and F) are images after 24 h of transfection. Plasmid DNA labeled with cyanine 5 (red) was used. The cell nuclei were stained with Hoechst 33342 (blue), and the late endosome and lysosome were stained with LysoTracker Green (green). Each scale bar represents 20 μm.

In summary, we have developed ternary polyplexes that express negative charges at the pH value of the cell exterior and that turn positive to disrupt the endosome at endosomal pH values. Eventually, these polyplexes achieved appreciably high transfection activity and low toxicity against sensitive primary cells (HUVEC). The transfection efficiency of this ternary polyplex system could be enhanced more by the conjugation of appropriate ligands, such as an RGD peptide for active internalization through binding of the integrin receptor.[12] The concept of our charge-conversion ternary polyplex with an endosome-disrupting moiety could easily be applied to various sensitive primary cells, the efficient and non-chemotoxic transfection of which is one of the most important and urgent issues in the biomedical field. Also, the stability of the ternary polyplex in the presence of negatively

charged serum proteins could be helpful for the development of in vivo gene vectors.

Received: February 28, 2008
Revised: April 10, 2008
Published online: June 4, 2008

Keywords: charge conversion · DNA · gene delivery · polymers · transfection

[1] a) D. W. Pack, A. S. Hoffman, S. Pun, P. S. Stayton, *Nat. Rev. Drug Discovery* **2005**, *4*, 581–593; b) E. Mastrobattista, M. A. E. M. Aa, W. E. Hennink, D. J. A. Crommelin, *Nat. Rev. Drug Discovery* **2006**, *5*, 115–121.

[2] a) O. Boussif, F. Lezoualc'h, M. A. Zanta, M. D. Mergny, D. Scherman, B. Demeneix, J. P. Behr, *Proc. Natl. Acad. Sci. USA* **1995**, *92*, 7297–7301; b) M. Neu, D. Fischer, T. Kissel, *J. Gene Med.* **2005**, *7*, 992–1009.

[3] a) M. X. Tang, C. T. Redemann, F. C. Szoka, *Bioconjugate Chem.* **1996**, *7*, 703–714; b) R. Wattiaux, N. Laurent, S. W.-D. Coninck, M. Jadot, *Adv Drug Delivery Rev.* **2000**, *41*, 201–208.

[4] a) A. C. Hunter, *Adv. Drug Delivery Rev.* **2006**, *58*, 1523–1531; b) M. Ogris, S. Brunner, S. Schüler, R. Kircheis, E. Wagner, *Gene Ther.* **1999**, *6*, 595–605.

[5] V. S. Trubetskoy, S. C. Wong, V. Subbotin, V. G. Budker, A. Loomis, J. E. Hagstrom, J. A. Wolff, *Gene Ther.* **2003**, *10*, 261–271.

[6] M. Han, Y. Bae, N. Nishiyama, K. Miyata, M. Oba, K. Kataoka, *J. Controlled Release* **2007**, *121*, 38–48.

[7] a) E. R. Gillies, A. P. Goodwin, J. M. Fréchet, *Bioconjugate Chem.* **2004**, *15*, 1254–1263; b) M. Krämer, J. F. Stumbé, H. Türk, S. Krause, A. Komp, L. Delineau, S. Prokhorova, H. Krautz, R. Haag, *Angew. Chem.* **2002**, *114*, 4426–4431; *Angew. Chem. Int. Ed.* **2002**, *41*, 4252–4256.

[8] a) Y. Lee, S. Fukushima, Y. Bae, S. Hiki, T. Ishii, K. Kataoka, *J. Am. Chem. Soc.* **2007**, *129*, 5362–5363; b) D. B. Rozema, D. L. Lewis, D. H. Wakefield, S. C. Wong, J. J. Klein, P. L. Roesch, S. L. Bertin, T. W. Reppen, Q. Chu, A. V. Blokhin, J. E. Hagstrom, J. A. Wolff, *Proc. Natl. Acad. Sci. USA* **2007**, *104*, 12982–12987.

[9] a) N. Kanayama, S. Fukushima, N. Nishiyama, K. Itaka, W.-D. Jang, K. Miyata, Y. Yamasaki, U.-I. Chung, K. Kataoka, *ChemMedChem* **2006**, *1*, 439–444; b) K. Masago, K. Itaka, N. Nishiyama, U. Chung, K. Kataoka, *Biomaterials* **2007**, *28*, 5169–5175.

[10] a) V. Zaric, D. Weltin, P. Erbacher, J. S. Remy, J. P. Behr, D. Stephan, *J. Gene Med.* **2004**, *6*, 176–184; b) J. J. Green, G. T. Zugates, N. C. Tedford, Y. H. Huang, L. G. Griffith, D. A. Lauffenburger, J. A. Sawicki, R. Langer, D. G. Anderson, *Adv. Mater.* **2007**, *19*, 2836–2842.

[11] a) D. Fischer, Y. Li, B. Ahlemeyer, J. Krieglstein, T. Kissel, *Biomaterials* **2003**, *24*, 1121–1131; b) S. M. Moghimi, P. Symonds, J. C. Murray, A. C. Hunter, G. Debska, A. Szewczyk, *Mol. Ther.* **2005**, *11*, 990–995.

[12] a) K. Temming, R. M. Schiffelers, G. Molema, R. J. Kok, *Drug Resist. Updates* **2005**, *8*, 381–402; b) M. Oba, S. Fukushima, N. Kanayama, K. Aoyagi, N. Nishiyama, H. Koyama, K. Kataoka, *Bioconjugate Chem.* **2007**, *18*, 1415–1423.

J|A|C|S
ARTICLES

Published on Web 04/09/2008

PEG-Detachable Polyplex Micelles Based on Disulfide-Linked Block Catiomers as Bioresponsive Nonviral Gene Vectors

Seiji Takae,[†] Kanjiro Miyata,[‡,⊥] Makoto Oba,[§] Takehiko Ishii,[‡,⊥] Nobuhiro Nishiyama,[||,⊥] Keiji Itaka,[||] Yuichi Yamasaki,[†,⊥] Hiroyuki Koyama,[§] and Kazunori Kataoka*[,†,‡,||,⊥]

Department of Materials Engineering, Graduate School of Engineering, The University of Tokyo, 7-3-1 Hongo, Bunkyo-ku, Tokyo 113-8656, Japan, Department of Bioengineering, Graduate School of Engineering, The University of Tokyo, 7-3-1 Hongo, Bunkyo-ku, Tokyo 113-8656, Japan, Department of Clinical Vascular Regeneration, Graduate School of Medicine, The University of Tokyo, 7-3-1 Hongo, Bunkyo-ku, Tokyo 113-8655, Japan, Division of Clinical Biotechnology, Center for Disease Biology and Integrative Medicine, Graduate School of Medicine, The University of Tokyo, 7-3-1 Hongo, Bunkyo-ku, Tokyo 113-0033, Japan, and Center for NanoBio Integration, The University of Tokyo, 7-3-1 Hongo, Bunkyo-ku, Tokyo 113-8656, Japan

Received January 15, 2008; E-mail: Kataoka@bmw.t.u-tokyo.ac.jp

Abstract: PEG-based polyplex micelles, which can detach the surrounding PEG chains responsive to the intracellular reducing environment, were developed as nonviral gene vectors. A novel block catiomer, PEG-SS-P[Asp(DET)], was designed as follows: (i) insertion of biocleavable disulfide linkage between PEG and polycation segment to trigger PEG detachment and (ii) a cationic segment based on poly(aspartamide) with a flanking *N*-(2-aminoethyl)-2-aminoethyl group, P[Asp(DET)], in which the Asp(DET) unit acts as a buffering moiety inducing endosomal escape with minimal cytotoxicity. The polyplex micelles from PEG-SS-P[Asp(DET)] and plasmid DNA (pDNA) stably dispersed in an aqueous medium with a narrowly distributed size range of ~80 nm due to the formation of hydrophilic PEG palisades while undergoing aggregation by the addition of 10 mM dithiothreitol (DTT) at the stoichiometric charge ratio, indicating the PEG detachment from the micelles through the disulfide cleavage. The PEG-SS-P[Asp(DET)] micelles showed both a 1–3 orders of magnitude higher gene transfection efficiency and a more rapid onset of gene expression than PEG-P[Asp(DET)] micelles without disulfide linkages, due to much more effective endosomal escape based on the PEG detachment in endosome. These findings suggest that the PEG-SS-P[Asp(DET)] micelle may have promising potential as a nonviral gene vector exerting high transfection with regulated timing and minimal cytotoxicity.

Introduction

Successful gene therapy, which is a promising treatment for numerous intractable diseases, relies on the development of efficient gene vectors. Polyplexes formed by electrostatic interaction between plasmid DNA (pDNA) and cationic polymers (catiomers) have attracted much attention as a safe, versatile alternative to viral vectors.[1–7] A promising approach to realizing the polyplexes for in vivo gene delivery is the use of PEG-based block catiomers. These catiomers spontaneously associate with pDNA to form sub-100 nm polyplex micelles with a dense, hydrophilic PEG palisade surrounding the core.[8–11] These micelles show high colloidal stability under physiological conditions and substantial transfection activity against various cell types even after preincubation with serum proteins.[12,13] Moreover, polyplex micelles demonstrate prolonged blood circulation and in vivo gene transfer to the liver and tumor.[14–16]

[†] Department of Materials Engineering, The University of Tokyo.
[‡] Department of Bioengineering, The University of Tokyo.
[§] Department of Clinical Vascular Regeneration, The University of Tokyo.
[||] Center for Disease Biology and Integrative Medicine, The University of Tokyo.
[⊥] Center for NanoBio Integration, The University of Tokyo.

(1) Pack, D. W.; Hoffman, A. S.; Pun, S.; Stayton, P. S. *Nat. Rev. Drug Discov.* **2005**, *4*, 581–593.
(2) Merdan, T.; Kopecek, J.; Kissel, T. *Adv. Drug Delivery Rev.* **2002**, *54*, 715–758.
(3) Wagner, E.; Meyer, M. *Hum. Gene Ther.* **2006**, *17*, 1062–1076.
(4) Kabanov, A. V. *Adv. Drug Delivery Rev.* **2006**, *58*, 1597–1621.
(5) Park, T. G.; Jeong, J. H.; Kim, S. W. *Adv. Drug Delivery Rev.* **2006**, *58*, 467–486.
(6) Osada, K.; Kataoka, K. *Adv. Polym. Sci.* **2006**, *202*, 113–153.
(7) Neu, M.; Fischer, D.; Kissel, T. *J. Gene Med.* **2005**, *7*, 992–1009.
(8) Katayose, S.; Kataoka, K. *Bioconjugate Chem.* **1997**, *8*, 702–707.
(9) Katayose, S.; Kataoka, K. *J. Pharm. Sci.* **1998**, *87*, 160–163.
(10) Ogris, M.; Brunner, S.; Schuller, S.; Kircheis, S.; Wagner, E. *Gene Ther.* **1999**, *6*, 595–605.
(11) Kwok, K. Y.; McKenzie, D. L.; Evers, D. L.; Rice, K. G. *J. Pharm. Sci.* **1999**, *88*, 996–1003.
(12) Itaka, K.; Yamauchi, K.; Harada, A.; Nakamura, K.; Kawaguchi, H.; Kataoka, K. *Biomaterials* **2003**, *24*, 4495–4506.
(13) Itaka, K.; Harada, A.; Nakamura, K.; Kawaguchi, H.; Kataoka, K. *Biomacromolecules* **2002**, *3*, 841–845.
(14) Harada-Shiba, M.; Yamauchi, K.; Harada, A.; Takanisawa, I.; Shimokado, K.; Kataoka, K. *Gene Ther.* **2002**, *9*, 407–414.
(15) Miyata, K.; Kakizawa, K.; Nishiyama, N.; Yamasaki, Y.; Watanabe, T.; Kohara, M.; Kataoka, K. *J. Controlled Release* **2005**, *109*, 15–23.

10.1021/ja800336v CCC: $40.75

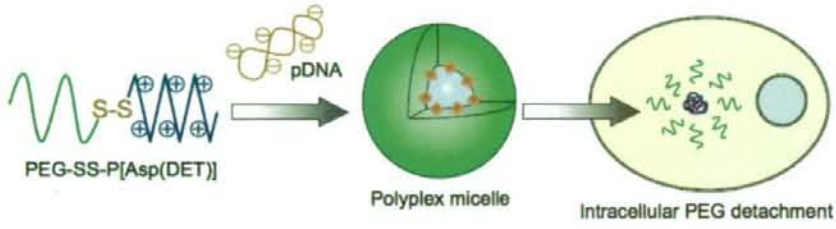

Figure 1. Schematic illustration of PEG-detachable polyplex micelle formation and the PEG detachment in the reducing intracellular environment.

We recently reported high transfection efficiency and low cytotoxicity with the use of polyplex micelles formed by PEG-*block*-poly(aspartamide) copolymers carrying the *N*-(2-aminoethyl)-2-aminoethyl group in the side chain (PEG-P[Asp(DET)]).[17] With regard to in vivo application, the polyplex micelles demonstrate appreciable gene transfer into vascular lesions without any vessel occlusion by thrombus[18] and bone regeneration of a mouse bone defect when transfected with genes coding for osteogenic factors.[19] These successful in vivo gene therapies have been explained by the specific structure of the side chain of P[Asp(DET)], in which the 1,2-ethanediamine moiety of the *N*-(2-aminoethyl)-2-aminoethyl group exhibits a distinct two-step protonation behavior, suggesting a potential proton sponge capacity of Asp(DET) units for efficient endo/lysosomal escape.[17]

However, polyplex micelles formed from PEG-P[Asp(DET)] could be further improved upon to achieve successful in vivo systemic therapies. P[Asp(DET)] homopolymer polyplexes show higher transfection efficiency than PEG-P[Asp(DET)] micelles especially at low charge ratios,[20] suggesting that the PEG palisade surrounding PEG-P[Asp(DET)] polyplex micelles would hamper the transfection. The decrease in gene transfection efficiency by PEGylation to catiomers (PEG dilemma) is also observed in previous work.[16,21,22] In addition, the time-dependent monitoring of gene expression against multicellular tumor spheroids reveals that the polyplex micelles from PEG-P[Asp(DET)] cause delayed gene expression, compared with polyplexes from cationic homopolymers.[20] This is sometimes undesired especially when rapid expression is required. On the other hand, the polyplexes from P[Asp(DET)] homocatiomers tend to aggregate through interactions with serum proteins,[18] suggesting limited in vivo application of the system without PEGylation. Although P[Asp(DET)] homocatiomers exhibited appreciably lower cytotoxicity compared with typical polycations such as polyethyleneimine (PEI),[23] PEGylation to P[Asp(DET)] further decreases the cytotoxicity to obtain successful transfection of primary cells.[17,18,20]

In order to overcome the aforementioned PEG dilemma, we designed here PEG detachable smart polyplex micelles sensitive to the intracellular environment as a smart gene vector (Figure 1). Block catiomers containing disulfide linkages between PEG and P[Asp(DET)] segments, PEG-SS-P[Asp(DET)], were synthesized to obtain this design goal (Scheme 1). Subsequent disulfide reduction of the block catiomer can occur during several steps of the endocytic pathway.[24] The cytoplasm and nuclear space are highly reducing environments due to abundant reduced glutathione (GSH) as well as redox enzymes such as the thioredoxin family. In addition, several studies suggest that disulfide bond reduction can begin on the exofacial surface of the cell and must continue after endocytosis. In this regard, involvement of plasma membrane-associated protein disulfide isomerase (PDI) is strongly implicated, as disulfide reduction is inhibited by an anti-PDI antibody and a PDI-inhibitor.[25,26] Moreover, NADH-oxidase (NOX) is reported as another cell surface-associated protein with disulfide−thiol interchange activity similar to PDI. Interestingly, the activity of this enzyme is constitutively activated in cancerous cells such as HeLa and hepatoma cells.[27] Finally, cysteine is actively transported from the cytoplasm to the lysosome lumen via a specific transporter in fibroblasts.[28]

Though the cleavage mechanism of the disulfide linkages cannot be predicted for the PEG-SS-P[Asp(DET)] micelle system utilized herein, the effect of PEG detachment on the gene transfection efficiency can be predicted based on where cleavage may occur. As a result of PEG detachment at the cell surface, the exposed cation segments may trigger a strong association to cells, increasing the cellular uptake of the micelles. Inside endosomes, the PEG detachment would cause the interaction between the exposed cation segments and the endosomal membrane and/or increase endosomal pressure, resulting in the destruction of the endosomal membrane to enable effective endosomal escape. In the cytoplasm and nucleus, the release of pDNA that forms the polyplex core might become smoother because steric repulsion disappears as the PEG cleaves, causing easier access of cellular polyanions to the complex core. Even if the reduction of disulfide linkages occurs in any of the steps outlined above, a more rapid alteration of gene expression and an increased transfection efficiency are expected.

(16) Kursa, M.; Walker, G. F.; Roessler, V.; Ogris, M.; Roedl, W.; Kircheis, R.; Wagner, E. *Bioconjugate Chem.* **2003**, *14*, 222–231.
(17) Kanayama, N.; Fukushima, S.; Nishiyama, N.; Itaka, K.; Jang, W.-D.; Miyata, K.; Yamasaki, Y.; Chung, U.-i.; Kataoka, K. *ChemMedChem* **2006**, *1*, 439–444.
(18) Akagi, D.; Oba, M.; Koyama, H.; Nishiyama, N.; Fukushima, S.; Miyata, T.; Nagawa, H.; Kataoka, K. *Gene Ther.* **2007**, *14*, 1029–1038.
(19) Itaka, K.; Ohba, S.; Miyata, K.; Kawaguchi, H.; Nakamura, K.; Takato, T.; Chung, U.-i.; Kataoka, K. *Mol. Ther.* **2007**, *15*, 1655–1662.
(20) Han, M.; Bae, Y.; Nishiyama, N.; Miyata, K.; Oba, M.; Kataoka, K. *J. Controlled Release* **2007**, *121*, 38–48.
(21) Brissault, B.; Kichler, A.; Leborgne, C.; Danos, O.; Cheradame, H.; Gau, J.; Auvray, L.; Guis, C. *Biomacromolecules* **2006**, *7*, 2863–2870.
(22) Sagara, K.; Kim, S. W. *J. Controlled Release* **2002**, *79*, 271–281.
(23) Masago, K.; Itaka, K.; Nishiyama, N.; Chung, U.-i.; Kataoka, K. *Biomaterials* **2007**, *28*, 5169–5175.
(24) Saito, G.; Swanson, J. A.; Lee, K.-D. *Adv. Drug Delivery Rev.* **2003**, *55*, 199–215.
(25) Feener, E. P.; Shen, W. C.; Ryser, H. J. *J. Biol. Chem.* **1990**, *265*, 18780–18785.
(26) Mandel, R.; Ryser, H. J.; Ghani, F.; Wu, M.; Peak, D. *Proc. Natl. Acad. Sci. U.S.A.* **1993**, *90*, 4112–4116.
(27) Morre, D. J.; Morre, D. M. *Free Radical Res.* **2003**, *37*, 795–808.
(28) Pisoni, R. L.; Acker, T. L.; Lisowski, K. M.; Lemons, R. M.; Thoene, J. G. *J. Cell Biol.* **1990**, *110*, 327–335.

Scheme 1. Synthetic Route of PEG-SS-P[Asp(DET)] Synthesis (Left) and the Chemical Structures of Control Polymers Used in This Experiment (PEG-P[Asp(DET)] and P[Asp(DET)]) (Right)

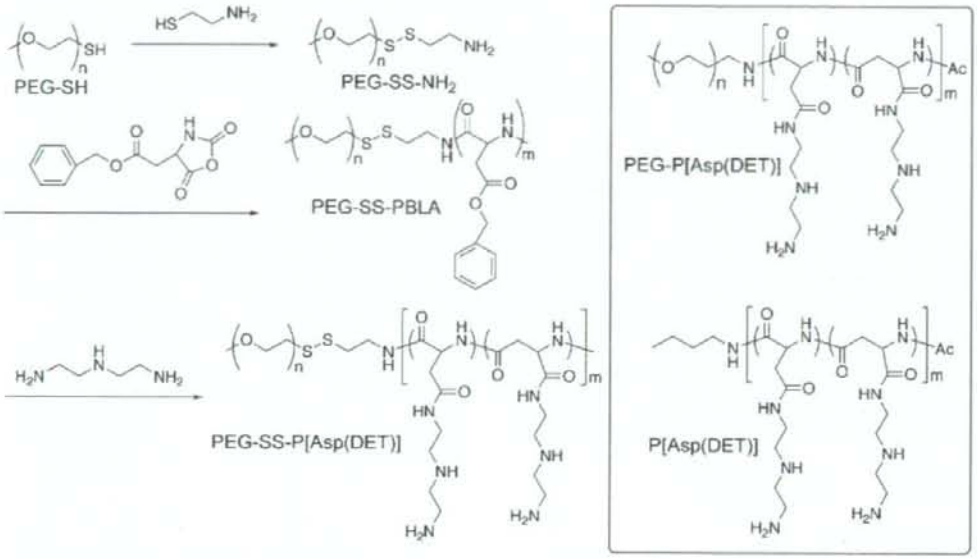

Based on such assumptions, we newly synthesized the PEG-SS-P[Asp(DET)] copolymer and prepared polyplex micelles sensitive to reducing environments. These micelles were expected to show comparable colloidal stability to PEG-P[Asp(DET)] micelles before cellular uptake, while, inside the cell, detachment of PEG would enable pDNA activity and alteration to gene expression. Therefore, careful characterization of both the PEG-SS-P[Asp(DET)] copolymer and the polyplex micelles was performed in regards to the reduction of disulfide linkages. In addition, the influence of the PEG detachment on the onset of gene expression and the mechanism of the disulfide reduction were evaluated through the time-dependent observation of the gene expression and the intracellular localization of pDNA.

Materials and Methods

Materials. α-Methoxy-ω-mercapto PEG (PEG-SH, $M_n = 10000$, $M_w/M_n = 1.03$) and β-benzyl-L-aspartate *N*-carboxyanhydride (BLA-NCA) were obtained from NOF Co. (Tokyo, Japan). Methanol (MeOH), 2-aminoethanethiol, benzene, acetonitrile, hexane, ethyl acetate, and D-luciferin were purchased from Wako Chemical Industries, Ltd. (Osaka, Japan). Dichloromethane, *N,N*-dimethylformamide (DMF), diethylenetriamine (DET), and *N*-methyl-2-pyrrolidone (NMP) were also purchased from Wako Chemical Industries and purified by distillation before use. A pGL3 control vector, which was purchased from Promega Co. (Madison, WI), was used as pDNA in all the experiments. This pDNA was amplified in competent DH5α *Escherichia coli* and purified using HiSpeed Plasmid MaxiKit purchased from QIAGEN Inc. (Valencia, CA). Water was purified using a Milli-Q instrument (Millipore, Bedford, MA).

Synthesis of PEG-SS-P[Asp(DET)]. As shown in Scheme 1, PEG-SH (1 g, 0.1 mmol) was dissolved in MeOH (100 mL), followed by the reaction with 2-aminoethanethiol (100 equiv to PEG-SH, 0.77 g, 10 mmol) at room temperature to obtain PEG-SS-NH_2. After a GPC peak due to PEG dimers (PEG-SS-PEG) generated by the side reaction disappeared, the reaction mixture was dialyzed against MeOH for 2 days and evaporated. Then, 80 mL of benzene were added, and the mixture was freeze-dried to obtain the white powder. To remove the PEG disulfide dimers (PEG-SS-PEG) generated during the dialysis, the powder dissolved in 30 mL of H_2O/CH_3CN (4:1) was loaded onto a CM Sephadex C-50 cation exchange chromatograph (GE Healthcare UK, Ltd., Little Chalf-ont, England), eluted with H_2O/CH_3CN (4:1) containing 0.125% NH_3. The eluate was evaporated and freeze-dried with distilled water to obtain the PEG-SS-NH_2 (570 mg, 57% yield). From gel permeation chromatography (GPC), M_n and M_w/M_n were determined to be 9880 and 1.02, respectively. The conversion to the aminoethanethiol moiety was confirmed to be quantitative (94%) based on the ^{1}H NMR data [CH_3 (3.2 ppm) and CH_2 (2.8 ppm)] (Figure S1) measured with a JEOL EX300 spectrometer (JEOL, Tokyo, Japan).

The PEG-SS-poly(β-benzyl L-aspartate) (PEG-SS-PBLA) copolymer was prepared by the ring opening polymerization of BLA-NCA (4.4 mmol, 1.1 g) in CH_2Cl_2/DMF (10:1, 15 mL) at 35 °C from the terminal primary amino group of PEG-SS-NH_2 (0.04 mmol, 400 mg).[29] The reaction mixture was precipitated into hexane/AcOEt (6:4). After filtration, the precipitate was dissolved in a small amount of CH_2Cl_2, followed by the addition of an excess amount of benzene, and lyophilized to obtain the white powder (910 mg, 61% yield). The degree of polymerization (DP) of PBLA was calculated to be 100 from ^{1}H NMR spectroscopy based on the peak intensity of benzyl protons of PBLA side chains (7.3 ppm) to the methylene protons of the PEG chain (3.6 ppm) (Figure S2).

Lyophilized PEG-SS-PBLA (130 mg) was dissolved in NMP (5.2 mL) at 27 °C, followed by the reaction with DET (2.3 mL, 50 equiv to benzyl group of PBLA segment) diluted in NMP (2.3 mL) under anhydrous conditions at 15 °C. After 15 min, the reaction mixture was slowly added dropwise into an aqueous solution of acetic acid (10% v/v, 40 mL) and dialyzed against a solution of 0.01 N HCl and, subsequently, distilled water (MWCO: 6–8000 Da). The final solution was lyophilized to obtain the polymer as the chloride salt form with a yield of 66% (104 mg). The structure of this block cationer was confirmed by ^{1}H NMR and size-exclusion chromatography (SEC) [column: Superdex 200 10/300 GL (GE Healthcare UK, Ltd.); eluent: 10 mM Tris-HCl buffer + 500 mM NaCl (pH 7.4); flow rate: 0.75 mL/min; detector RI; ambient temperature].

(29) Harada, A.; Kataoka, K. *Macromolecules* **1995**, *28*, 5294–5299.

Preparation of PEG-SS-P[Asp(DET)]/pDNA Polyplex Micelles. The PEG-SS-P[Asp(DET)] block copolymer and pDNA were separately dissolved in 10 mM Tris-HCl buffer (pH 7.4). The polymer solution was added to a 2-times-excess volume of 50 μg/mL pDNA solution to form the polyplex micelles at various *N/P*, the residual molar ratio of the amino group in the block cationer to phosphate group in pDNA. The final concentration of pDNA in all the samples was adjusted to 33 μg/mL. The PEG-P[Asp(DET)] block copolymer (M_w = 39 000; DP of P[Asp(DET)] segment: 100) and P[Asp(DET)] (DP = 98) (Scheme 1) were used as controls, and their polyplexes were prepared in the same way as PEG-SS-P[Asp(DET)]/pDNA polyplex micelles.

Gel Retardation Assay. Polyplex solutions formed with pDNA (33 μg/mL) were diluted to 20 μg/mL with 10 mM Tris-HCl buffer and then electrophoresed at 100 V for 1 h on a 0.9 wt% agarose gel in 3.3 mM Tris-acetic acid buffer containing 1.7 mM sodium acetate. The migrated pDNA was visualized with ethidium bromide staining (0.5 μg/mL in deionized water).

Dynamic Light Scattering (DLS) Measurements. The size of the polyplexes was evaluated by DLS. Sample solutions with various *N/P* ratios in 10 mM Tris-HCl buffer (pH 7.4) were adjusted to have a pDNA concentration of 33 μg/mL. DLS measurements were carried out at 37 °C using a Zetasizer Nano-ZS instrument (Malvern Instruments, Malvern, UK), equipped with a He−Ne ion laser (λ = 633 nm) with a scattering angle of 90°.

Radiolabeling of pDNA and Cellular Uptake Study of the Polyplexes. pDNA was radioactively labeled with ^{32}P-dCTP using the Nick Translation System (Invitrogen Co., Carlsbad, CA). Unincorporated nucleotides were removed using the High Pure PCR Product Purification Kit (Roche Diagnostics Co., Indianapolis, IN). After the purification, 7 μg of labeled pDNA were mixed with 700 μg of nonlabeled pDNA. The polyplex and micelle samples were prepared by mixing the radioactive pDNA solution with each polymer solution (33 μg pDNA/mL). For the cellular uptake experiment, HeLa cells were seeded in Dulbecco's modified Eagle medium (DMEM) containing 10% fetal bovine serum (FBS) on 24-well tissue culture treated plates 24 h prior to experimentation. The cells were incubated with 30 μL of the radioactive polyplex solution (1 μg of pDNA/well) in 400 μL of DMEM containing 10% FBS. After 6 h of incubation, the cells were washed 3 times with PBS and lysed with 200 μL of cell culture lysis buffer (Promega, Co., Madison, WI). The lysates were mixed with 5 mL of scintillation cocktail, Ultima Gold (PerkinElmer, MA), and then, the radioactivity was measured using a liquid scintillation counter. The results are presented as a mean and standard deviation of the mean obtained from four samples.

In Vitro Transfection. HeLa cells were seeded on 24-well culture plates and incubated for 24 h in 400 μL of DMEM containing 10% FBS before transfection. The cells were then incubated with the polyplex micelles prepared from PEG-SS-P[Asp(DET)], PEG-P[Asp(DET)], and P[Asp(DET)] (30 μL, 1 μg of pDNA/well) with various *N/P* ratios in DMEM containing 10% FBS for 6 h, followed by an additional incubation for 42 h in the absence of polyplexes. The cells were washed in triplicate with 200 μL of Dulbecco's PBS and lysed by the addition of 400 μL/well of the Promega lysis buffer. Luciferase gene expression was evaluated using the Luciferase Assay System (Promega Co., Madison, WI) and a Lumat LB957 luminometer (Berthold Technologies Co., Bad Wildbad, Germany). The results were expressed as light units per milligram of cell protein determined by a BCA assay kit (PIERCE Biotechnology, Rockford, IL). The results are presented as a mean and standard deviation of the mean obtained from four samples.

Time-Dependent Monitoring of in Vitro Transfection. HeLa cells and 293T cells were seeded on 35-mm culture dishes and incubated for 24 h in 2 mL of DMEM containing 10% FBS before transfection. The cells were then incubated with the polyplex micelles prepared from PEG-SS-P[Asp(DET)], PEG-P[Asp(DET)], and P[Asp(DET)] (90 μL/dish, 3 μg of pDNA/dish) at *N/P* = 32 in DMEM containing 10% FBS. After 6 h, the medium was exchanged with fresh media containing 100 μM D-luciferin. The dishes were set in a luminometer incorporated in a small CO_2 incubator (AB-2550 Kronos Dio, ATTO Co., Tokyo, Japan), and the bioluminescence was monitored every 20 min (2 min collection time).

Confocal Laser Scanning Microscope (CLSM) Observation. pDNA was labeled with Cy5 using the Label IT Nucleic Acid Labeling Kit (Mirus, Madison, WI) according to the manufacture's protocol. HeLa cells were seeded on a 35-mm glass base dish (Iwaki, Japan) and incubated overnight in 1 mL of DMEM containing 10% FBS. After the medium was replaced with fresh medium, 90 μL of polyplex solution containing 3 μg of Cy5-labeled pDNA (*N/P* = 32) were applied. After 6 h of incubation, the medium was removed, the cells were washed twice with PBS, and fresh media was added. The intracellular distributions of the polyplex micelles were observed by CLSM following acidic late endosome and lysosome staining with LysoTracker Green (Molecular Probes, Eugene, OR). The CLSM observation was performed using LSM 510 (Carl Zeiss, Germany) with a 63× objective (C-Apochromat, Carl Zeiss, Germany) at excitation wavelengths of 488 nm (Ar laser) and 633 nm (He−Ne laser) for LysoTracker Green and Cy5, respectively. Colocalization of polyplex micelles in the late endosome and lysosome was quantified as follows:

Colocalization ratio = Cy5 pixels colocalization/Cy5 pixels total

where Cy5 pixels colocalization represents the number of pixels with Cy5 colocalizing with LysoTracker inside the cells and the Cy5 pixels total represents number of all pixels with Cy5 existing in the cells. The results are presented as a mean and standard error of the mean obtained from 10 cells.

Results and Discussion

Synthesis of PEG-SS-P[Asp(DET)]. A PEG-poly(aspartamide) block copolymer with a disulfide linkage between PEG and poly(aspartamide) was prepared as shown in Scheme 1. Initially, α-methoxy-ω-mercapto PEG (PEG-SH, M_n = 10 000) was reacted with 2-aminothanethiol in MeOH to introduce a primary amino group into PEG-SH via a disulfide linkage. The conversion ratio was confirmed to be 94% based on the ^{1}H NMR data (Figure S1). Then, β-benzyl L-aspartate *N*-carboxyanhydride (BLA-NCA) was polymerized in CH_2Cl_2/DMF at 35 °C by an initiation from the terminal primary amino group of PEG-SS-NH_2. The degree of polymerization (DP) of PBLA was calculated to be 100 from ^{1}H NMR spectroscopy, and GPC measurement revealed that the obtained PEG-SS-PBLA showed a unimodal molecular weight distribution (Figure S2). The aminolysis of PEG-SS-PBLA in NMP in the presence of a molar excess of diethylenetriamine (DET, 50 equiv relative to benzyl groups) was carried out. The ^{1}H NMR spectrum of the obtained polymer (Figure S3) reveals that the introduction of DET into the side chains of PBLA was almost quantitative (98.5%) in spite of the extremely short reaction time (15 min) and relatively low temperature (15 °C). The detailed mechanism of this unique aminolysis reaction of PBLA was reported elsewhere.[30] Size-exclusion chromatography (SEC) measurements revealed a unimodal molecular weight distribution of the obtained polymer (Figure 2, line 1), suggesting a minimal occurrence of inter- or intrapolymer cross-linking by DET during aminolysis. To confirm the presence of disulfide linkages between PEG and polycation segments, SEC measurement was done after the addition of 10 mM dithiothreitol (DTT) to the PEG-SS-P[Asp(DET)] solution. In the SEC chromatogram, two overlapping peaks (Figure 2, line 2) were observed at elution times extremely similar to those for PEG-SH (Figure 2, line 3) and

(30) Nakanishi, M.; Park, J.-S.; Jang, W.-D.; Oba, M.; Kataoka, K. *React. Funct. Polym.* **2007**, *67*, 1361–1372.

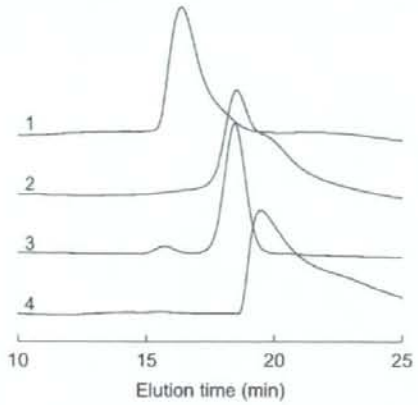

Figure 2. SEC charts of PEG-SS-P[Asp(DET)] (line 1), PEG-SS-P[Asp(DET)] after 4 h incubation with 10 mM DTT (line 2), PEG-SH (line 3), and P[Asp(DET)] (line 4).

P[Asp(DET)] (Figure 2, line 4), indicating that the obtained polymer was linked via a disulfide linkage between PEG and P[Asp(DET)] segments.

Formation of Polyplex Micelles from pDNA and PEG-SS-P[Asp(DET)]. Polyplex micelles were prepared by mixing each polymer solution with the pDNA solution at various *N*/*P* ratios. In order to demonstrate polyplex formation between PEG-SS-P[Asp(DET)] and pDNA, a gel electrophoresis retardation assay was performed using 0.9 wt % agarose gel. A PEG-P[Asp(DET)] block copolymer without the disulfide linkage and P[Asp(DET)] homocatiomer were used as controls (Scheme 1). As shown in Figure 3, the band of free pDNA disappeared at $N/P > 2$ in all of the samples, indicating successful and complete polyplex formation between pDNA and the three catiomers. This is stoichiometrically consistent with the monoprotonated form of the ethylenediamine unit in PEG-P[Asp(DET)] and P[Asp(DET)] at pH 7.4.[17,20] The diameters of the polyplexes or the polyplex micelles prepared at different *N*/*P* ratios are shown in Figure 4a. The diameters of the polyplex micelles from PEG-P[Asp(DET)] and PEG-SS-P[Asp(DET)] were determined to be 80–90 nm throughout the examined *N*/*P* ratios (1–16). On the other hand, the polyplexes from P[Asp(DET)] formed large aggregates with a size of approximately 600 nm specifically at $N/P \sim 2$. Considering that zeta-potential of the P[Asp(DET)] polyplex was close to neutral at $N/P = 2$ (Figure S4), the aggregation was presumably due to the formation of charge stoichiometric complexes showing lower electrostatic repulsion among the polyplexes. The system of PEG-SS-P[Asp(DET)] and PEG-P[Asp(DET)] did not show such aggregation, indicating a high colloidal stability due to the steric repulsion of the PEG palisades of the shell.[31]

Reducing Environment-Sensitive Cleavage of the Disulfide Linkages of the Polyplex Micelles from PEG-SS-P[Asp(DET)]. To confirm the detachment of PEG from the PEG-SS-P[Asp(DET)] polyplex micelles, the diameter of the micelles ($N/P = 2$) was monitored after the addition of 10 mM DTT, as a model reaction for the reducing environment of the cytoplasm. As shown in Figure 4b, 10 mM DTT rapidly induced an increase in size of PEG-SS-P[Asp(DET)] micelles, whereas, in the case of control

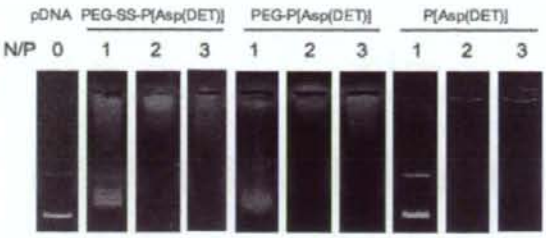

Figure 3. Gel retardation assay of the polyplexes.

micelles from PEG-P[Asp(DET)], such a size increase was not observed, indicating that the PEG chains on the PEG-SS-P[Asp(DET)] micelles were detached due to the cleavage of the disulfide bond. Moreover, as a model of the extracellular environment, the polyplex micelles were incubated in 10 μM DTT, which is an effective 50-fold molar equivalent of the PEG-SS-P[Asp(DET)] within the micelles. As a result, the polyplex micelles did not show increased size (Figure 4b), indicating that the PEG detachment would be dependent on the concentration of the surrounding thiol groups. To check the PEG detachment at other *N*/*P* ratios, the ζ-potential of the polyplex micelles was measured in the absence or presence of 10 mM DTT. The polyplexes from PEG-SS-P[Asp(DET)] and PEG-P[Asp(DET)] were observed to have ζ-potentials with a very small absolute value ($\sim$4 mV) in $N/P > 2$ (Figure S4), suggesting that the polyplexes from the PEG-*b*-catiomers form a core–shell micellar architecture with a hydrophilic and neutral PEG shell surrounding the polyplex core. After the addition of 10 mM DTT, the ζ-potential of PEG-SS-P[Asp(DET)] polyplex micelles shifted to a positive value ($\sim$28 mV) comparable to that of the P[Asp(DET)] polyplexes. On the other hand, there was no change in the ζ-potential of PEG-P[Asp(DET)] micelles by the addition of DTT. These results indicate that, regardless of *N*/*P* ratio, the surface-covered PEG chains detached from the PEG-SS-P[Asp(DET)] polyplex micelles when present in a reducing environment.

Cellular Uptake Study. Though the PEG-SS-P[Asp(DET)] polyplex micelles were responsive to reducing environments, it is significant to determine where the PEG chains will be detached after contact with cells. Rice et al. concluded that the complexes formed from PEG(5 kDa)-SS-Lys_{18} and pDNA showed more in vitro cellular uptake than PEG-Lys_{18} complexes without disulfide linkages, suggesting partial reduction of the disulfide linkages outside cells.[32] To confirm that the disulfide linkages were cleaved either outside or inside cells, polyplexes with ^{32}P-radiolabeled pDNA were prepared and the uptake to human cervical carcinoma HeLa cells was measured. As shown in Figure 5, PEG-SS-P[Asp(DET)] and PEG-P[Asp(DET)] polyplex micelles showed a minimal uptake into the cells, with only $\sim$0.5% of the total dose being taken up. In contrast, 2−4% of P[Asp(DET)] polyplexes were taken into the cells, probably due to the electrostatic association between the positive charge of the polyplexes and the negative charge of the plasma membrane. If the disulfide linkages were reduced prior to uptake by cells, a higher percentage of the PEG-SS-P[Asp(DET)] micelles would be taken up than the PEG-P[Asp(DET)] micelles. In contrast, the cellular uptakes of PEG-P[Asp(DET)] and PEG-SS-P[Asp(DET)] micelles are equivalent, suggesting that the

(31) Kataoka, K.; Harada, A.; Nagasaki, Y. *Adv. Drug Delivery Rev.* **2001**, *47*, 113–131.

(32) Kwok, K. Y.; McKenzie, D. L.; Evers, D. L.; Rice, K. G. *J. Pharm. Sci.* **1999**, *88*, 996–1003.

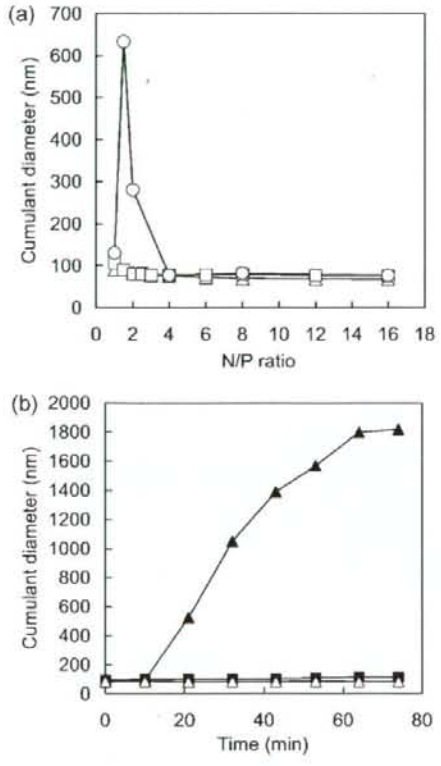

Figure 4. (a) Size of the polyplexes from PEG-SS-P[Asp(DET)] (△), PEG-P[Asp(DET)] (□), and P[Asp(DET)] (○). (b) Time-dependent change of the size of PEG-SS-P[Asp(DET)] polyplex micelles at $N/P = 2$ with 10 mM DTT (▲) and with 10 μM DTT (△), and PEG-P[Asp(DET)] polyplex micelles with 10 mM DTT (■).

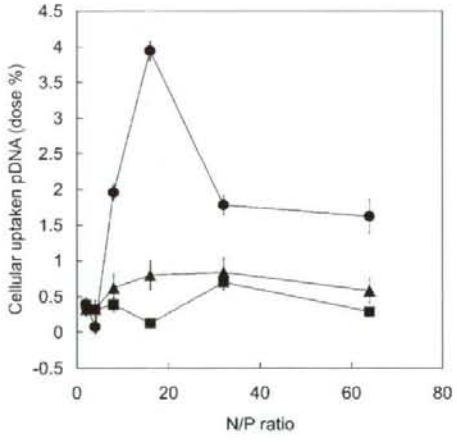

Figure 5. Cellular uptake of pDNA complexed with cationers; PEG-SS-P[Asp(DET)] (▲), PEG-P[Asp(DET)] (■), and P[Asp(DET)] (●). ^{32}P-labeled pDNA polyplexes were incubated with HeLa cells in DMEM containing 10% FBS at 37 °C for 6 h. The amount of internalized pDNA is represented as a percentage for the dosed pDNA (1 μg/well).

PEG-SS-P[Asp(DET)] micelles maintain their PEG palisade structure under normal culture conditions for at least 6 h. Note

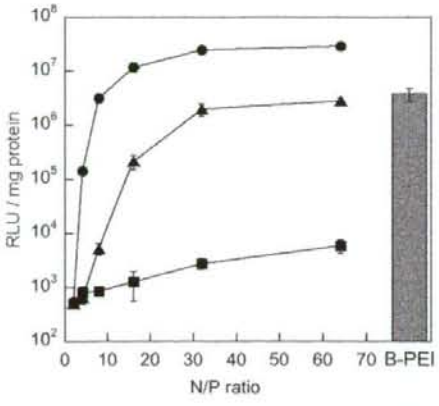

Figure 6. In vitro transfection of the luciferase gene into HeLa cells by polyplexes from PEG-SS-P[Asp(DET)] (▲), PEG-P[Asp(DET)] (■), and P[Asp(DET)] (●) with varying N/P ratios. Branched polyethyleneimine (B-PEI, 25 kDa) at $N/P = 32$ was shown as a control (gray bar). The cells were incubated with each polyplex in DMEM containing 10% FBS for 6 h, followed by incubation for a further 42 h in the absence of the polyplexes. Transfection is reported in relative light units (RLU) per mg of protein.

that there is a decrease in cellular uptake of the P[Asp(DET)] polyplexes with $N/P \geq 32$. This may be due to inhibition of uptake by free cationers which are not associated with the polyplexes.

In Vitro Transfection Efficiency and Cytotoxicity. The in vitro transfection efficiency of these polyplexes with HeLa cells was assessed using a luciferase assay. Based on the cellular uptake study, cells were incubated with the polyplexes for 6 h, followed by a 42 h incubation after medium replacement. As shown in Figure 6, PEG-SS-P[Asp(DET)] polyplex micelles showed 2–3 orders of magnitude higher transfection efficiency than the PEG-P[Asp(DET)] polyplex micelles at $N/P \geq 16$, which is comparable to branched polyethyleneimine (B-PEI, 25 kDa). It is surprising that the introduction of disulfide linkages to the block cationers remarkably increased the transfection efficiency, though the efficiency was somewhat less than P[Asp(DET)] polyplexes. Low cytotoxicity together with high transfection efficiency is an extremely important aspect for nonviral gene vectors. The cytotoxicity of the polyplexes was evaluated with the same cell culture procedure as the transfection, followed by the CellTiter-Glo luminescent cell viability assay. Polyplex micelles from PEG-SS-P[Asp(DET)], PEG-P[Asp(DET)], and P[Asp(DET)] polyplexes showed more than 90% cell viability in all N/P ratios tested in this study, while B-PEI polyplexes induced a significant decrease in cell viability (~40%) at $N/P = 64$ (Figure S5). A similar tendency was observed at lower N/P as well in the case of longer incubation times and higher doses (data not shown). These results indicate that P[Asp(DET)] and the block cationers would be desirable as in vivo gene vectors due to their high transfection efficiency as well as low toxicity.

Mechanism of the High Transfection Efficiency of PEG-SS-P[Asp(DET)] Micelles. It is important to understand where the disulfide linkages of the PEG-SS-P[Asp(DET)] polyplex micelles are cleaved inside the cell. Therefore, the time-dependent profile of transfection efficiency was monitored with AB-2550 Kronos Dio (ATTO Co. Ltd., Tokyo, Japan), which is a luminometer incorporated into a small CO_2 incubator, allowing continuous measurement of bioluminescence by transfected

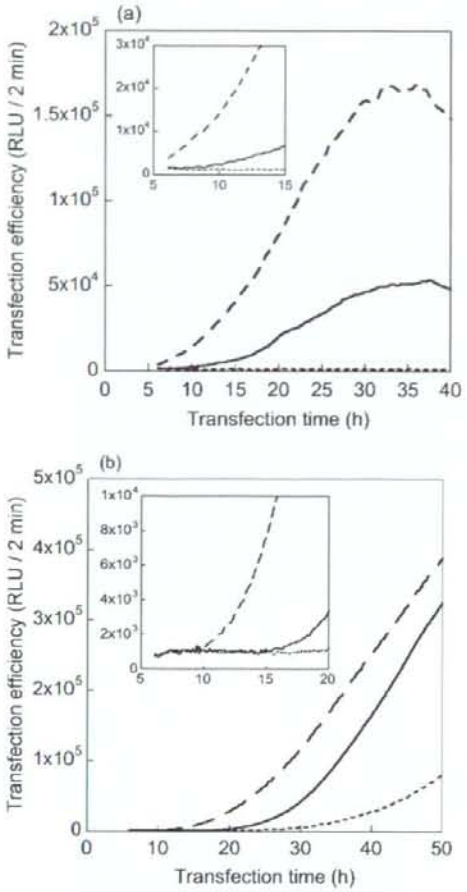

Figure 7. Time-dependent profiles of transfection efficiency against HeLa cells (a) and 293T cells (b) induced by PEG-SS-P[Asp(DET)] (solid line), PEG-P[Asp(DET)] (dotted line), and P[Asp(DET)] (dashed line) polyplexes at $N/P = 32$. The cells were incubated with each polyplex in DMEM containing 10% FBS for 6 h, followed by incubation in DMEM containing 10% FBS and 100 μM D-luciferin in the absence of polyplexes. The time shown in the x-axis started from the addition of polyplex solutions and the measurement started from 6 h. The inserts are expanded figures from 5 to 15 h (a) and from 5 to 20 h (b).

cells. After HeLa cells were incubated with the polyplexes for 6 h, the medium modified to include luciferin was used to culture the cells and bioluminescence from expressed luciferase was monitored at 20 min intervals. As shown in Figure 7a, the gene expression induced by P[Asp(DET)] polyplexes started to be observed immediately after the medium replacement (at 6 h), while the expression by PEG-SS-P[Asp(DET)] micelles started at 11 h and increased remarkably after 16 h. A similar tendency of delayed expression with PEG-SS-P[Asp(DET)] micelle carriers compared with P[Asp(DET)] polyplexes was observed with 293T cells as well (Figure 7b). The reason of the delayed expression of PEG-SS-P[Asp(DET)] micelles is presumably related to the process of the disulfide reduction inside the cell. In addition, clear expression by PEG-SS-P[Asp(DET)] micelles in 293T cells was observed 10 h earlier than PEG-P[Asp(DET)] micelles, probably due to the detachment of PEG chains. These results indicate that PEG-SS-P[Asp(DET)] micelles could regulate the onset of the gene expression, which is a significantly attractive characteristic in this system.

In order to gain more insight into the relationship between the cleavage of disulfide linkages and transfection efficiency, intracellular trafficking of pDNA in the micelles was observed with a confocal laser scanning microscope (CLSM), using PEG-SS-P[Asp(DET)] polyplex micelles with Cy5-labeled pDNA (red) at $N/P = 32$. LysoTracker (green) was used as an endo/lysosomal marker. As shown in Figure 8a, Cy5-pDNA of the polyplex micelles from PEG-P[Asp(DET)] and PEG-SS-P[Asp(DET)] associates to the plasma membrane 6 h after transfection, whereas the red fluorescence from P[Asp(DET)] polyplexes seemed to spread out from the green fluorescence of LysoTracker even at 6 h, indicating fast endosomal escape. This result would correspond to the transfection profile (Figure 7a) where transfection by P[Asp(DET)] polyplexes is observed starting at 6 h. Figure 8b shows CLSM images after 6 h of incubation with the polyplex and 6 h postincubation in the absence of polyplexes, corresponding to the time when a gene expression by PEG-SS-P[Asp(DET)] micelles started (12 h in Figure 7a). In these images, the pDNA of PEG-P[Asp(DET)] micelles is colocalized and sequestered in the endo/lysosome, resulting in the absence of expression in Figure 7a. On the other hand, the pDNA of PEG-SS-P[Asp(DET)] micelles spread out from LysoTracker, indicating that the PEG-SS-P[Asp(DET)] micelles that escaped from the endosome would be capable of inducing gene expression. In the case of P[Asp(DET)] polyplexes, pDNA spread out from endo/lysosome increased remarkably. Time-dependent colocalization of pDNA in the endo/lysosomes was quantified and is shown in Figure 8c. PEG-P[Asp(DET)] micelles exhibited high colocalization even after 2 days, while less colocalization was observed in the PEG-SS-P[Asp(DET)] system, suggesting a more effective endosomal escape. A similar localization profile of pDNA in the PEG-SS-P[Asp(DET)] system was observed in 293T cells (Figure S6). Considering the transfection profile as well as CLMS images (Figure 7 and 8), it is likely that cleavage of the disulfide linkages of PEG-SS-P[Asp(DET)] micelles occurs in the endocytic pathway, resulting in effective endosomal escape probably due to interaction between the exposed polycation segments and endosomal membrane, and/or increased osmotic pressure in the endosome induced by detached PEG chains. As a result, the gene expression onset of PEG-SS-P[Asp(DET)] micelles was intermediate when compared with P[Asp(DET)] polyplexes and PEG-P[Asp(DET)] micelles. There is an issue that disulfide reduction in the endosome would be disfavored due to the low GSH concentration as well as the acidic environment inducing protonation of thiol groups and decreased reactivity of thiol−disulfide oxidoreductase (e.g., PDI, thioredoxin, etc.) because these enzymes typically exhibit optimal activity around neutral pH. Nevertheless, Low et al. directly observed images of disulfide cleavage with FRET technology using folate−SS−rhodamine conjugates.[33] In addition, calcein-loaded polymersome formed from a PEG-SS-poly(propylene sulfide) block copolymer showed the rapid release of calcein inside the endosome due to the disulfide reduction, facilitating endosomal rupture.[34] In the case of the PEG-SS-P[Asp(DET)] system, considering the increased endosomal escape, not all PEG chains but a substantial fraction of them are assumed to be detached

(33) Yang, J.; Chen, H.; Vlahov, I. R.; Cheng, J.-X.; Low, P. S. *Proc. Natl. Acad. Sci. U.S.A.* **2006**, *103*, 13872–13877.
(34) Cerritelli, S.; Velluto, D.; Hubbell, J. A. *Biomacromolecules* **2007**, *8*, 1966–1972.

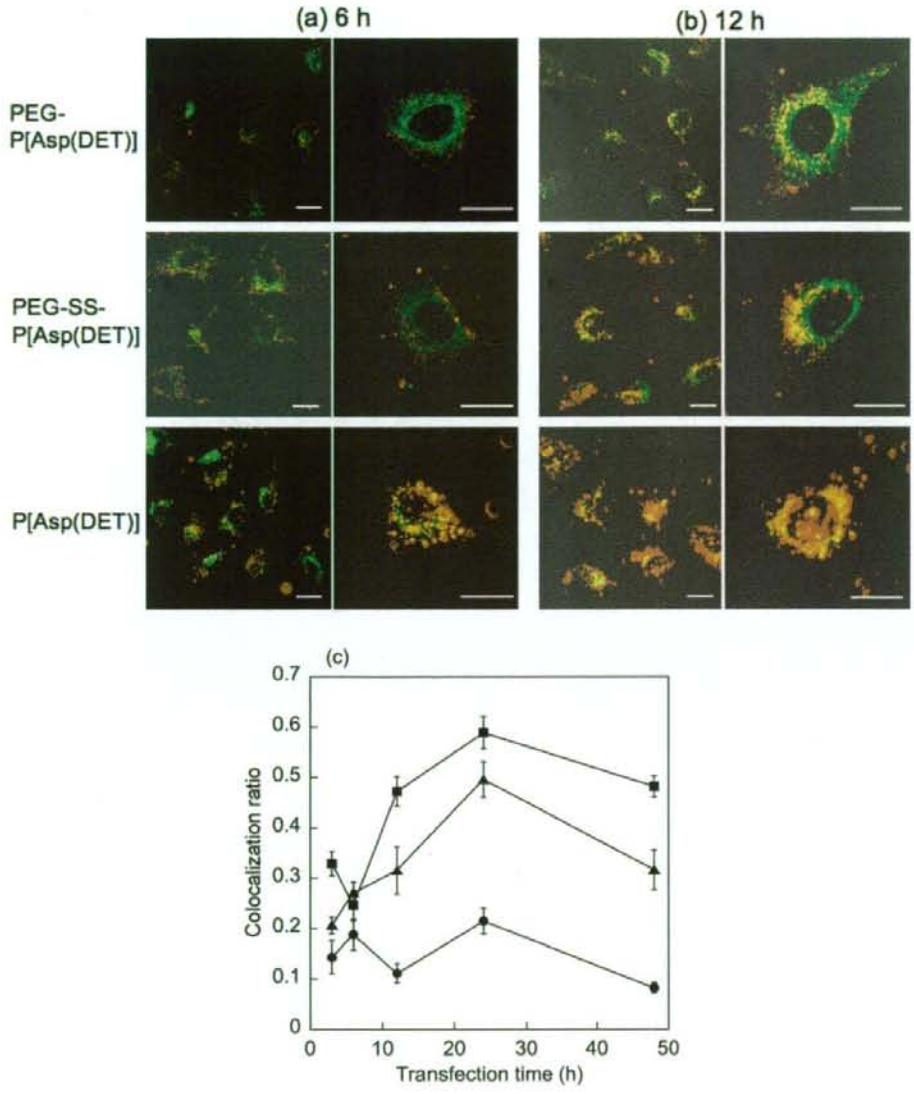

Figure 8. (a, b) Intracellular distribution of pDNA challenged by PEG-P[Asp(DET)] and PEG-SS-P[Asp(DET)] micelles, and P[Asp(DET)] polyplexes at $N/P = 32$. The complexes loaded with Cy5-labeled pDNA (red) were incubated with HeLa cells for 6 h, followed by incubation in the absence of polyplexes. The CLSM observation was performed 6 h (a) and 12 h (b) after transfection, using a 63× objective. The acidic late endosome and lysosome were stained with LysoTracker Green (green). The scale bar represents 20 μm. (c) Quantitative results of colocalization profile of Cy5-labeled pDNA in late endosome and lysosome transfected by PEG-P[Asp(DET)] (■), PEG-SS-P[Asp(DET)] (▲), and P[Asp(DET)] (●) polyplexes.

in the endocytic pathway as a result of disulfide reduction. In the future, further mechanistic investigations of the disulfide cleavage will be performed to reveal a detailed relationship between PEG detachment and gene transfection efficiency, contributing to establishing the design criteria for smart polyplex micelles useful for in vivo transfection studies.

Conclusion

We newly synthesized a disulfide-linked block catiomer, PEG-SS-P[Asp(DET)], to develop a PEG detachable polyplex micelle sensitive to an intracellular reducing environment. This micelle showed several orders of magnitude higher gene transfection efficiency than a micelle without disulfide linkages in spite of the similar level of their cellular uptakes. Moreover, gene expression induced by the PEG-SS-P[Asp(DET)] micelle started between the expression onsets of the P[Asp(DET)] polyplex and PEG-P[Asp(DET)] micelle, indicating that the PEG-SS-P[Asp(DET)] micelle could regulate the onset of the gene expression. CLSM images revealed that this transfection behavior of the PEG-SS-P[Asp(DET)] micelle could be explained by effective endosomal escape due to the PEG detachment in the endosome. As this micelle overcame the PEG dilemma, it would be highly promising for in vivo application to exert spatio-temporal regulated transfection with minimal cytotoxicity.

Acknowledgment. The authors acknowledge Mr. Shigeto Fukushima, the University of Tokyo, for his advice about polymer synthesis. This study was financially supported by the Core Research for Evolutional Science and Technology (CREST) from the Japan Science and Technology Agency (JST) and also by a grant for the 21st Century COE Program "Human-Friendly Materials based on Chemistry" from the Ministry of Education, Culture, Sports, Science and Technology of Japan (MEXT). S.T. would like to express his special gratitude for the scholarship from the Asahi Glass Scholarship Foundation.

Supporting Information Available: ^{1}H NMR spectra and GPC charts of PEG-SS-NH_2, PEG-SS-PBLA and PEG-SS-P[Asp-(DET)], ζ-potential measurements, cytotoxicity study, and CLSM images of 293T cells. These materials are available free of charge via the Internet at http://pubs.acs.org.

JA800336V

Photodynamic Therapy for Corneal Neovascularization Using Polymeric Micelles Encapsulating Dendrimer Porphyrins

Kenji Sugisaki,[1] *Tomohiko Usui,*[1] *Nobuhiro Nishiyama,*[2] *Woo-Dong Jang,*[3,4] *Yasuo Yanagi,*[1] *Satoru Yamagami,*[1] *Shiro Amano,*[1] *and Kazunori Kataoka*[3,4]

Purpose. To investigate the accumulation of new photosensitizers (PSs), dendrimer porphyrin (DP, free DP), and DP encapsulation into polymeric micelles (DP-micelle) and the efficacy of photodynamic therapy (PDT) in an experimental corneal neovascularization model in mice.

Methods. Corneal neovascularization was induced by suturing 10-0 nylon 1 mm away from the limbal vessel in C57BL6/J mice. To determine the accumulation of free DP and DP-micelle, 10 mg/kg free DP or DP-micelle was administered by intravenous injection 4 days after suture placement. Mice were killed 1, 4, 24, and 168 hours after the injection of PS. Twenty-four hours after the administration of free DP or DP-micelle, mice were treated with a diode laser of 438-nm wavelength at 10 or 50 J/cm^2. Fluorescein angiography was performed before and 7 days after irradiation, and the area of corneal neovascularization was quantified.

Results. Free DP and DP-micelle accumulated in the neovascularized area 1 hour to 24 hours after administration. Fluorescence of DP was weaker than that of DP-micelle. Neither DP-micelle nor DP could be detected in normal limbal vasculature. In the PDT experiments using PS, mean residual rates of corneal neovascularization were 10.1% in the mice treated with DP-micelle and 21.6% in the mice treated with free DP at 10 J/cm^2 ($P < 0.01$). At 50 J/cm^2, mean residual rates of corneal neovascularization were 10.6% in the mice treated with DP-micelle and 13.7% in the mice treated with free DP ($P > 0.05$). Although corneal neovascularization in PDT-treated mice exhibited significant regression compared with the control group, significant energy-related vessel regression with increasing laser energy could not be observed.

Conclusions. PDT with DP-micelle and free DP can provide efficacious treatment of corneal neovascularization. (*Invest Ophthalmol Vis Sci.* 2008;49:894-899) DOI:10.1167/iovs.07-0389

From the [1]Department of Ophthalmology, Faculty of Medicine, the [2]Department of Materials Engineering, Graduate School of Engineering, and the [3]Center for Disease Biology and Integrative Medicine, Graduate School of Medicine, University of Tokyo, Japan; and the [4]Department of Chemistry, College of Science, Yonsei University, Korea.

Supported in part by a Grant-in-Aid for Scientific Research from the Ministry of Education, Culture, Sports, Science and Technology of Japan.

Submitted for publication April 2, 2007; revised June 27, 2007; accepted January 25, 2008.

Disclosure: **K. Sugisaki**, None; **T. Usui**, None; **N. Nishiyama**, None; **W.-D. Jang**, None; **Y. Yanagi**, None; **S. Yamagami**, None; **S. Amano**, None; **K. Kataoka**, None

The publication costs of this article were defrayed in part by page charge payment. This article must therefore be marked "*advertisement*" in accordance with 18 U.S.C. §1734 solely to indicate this fact.

Corresponding author: Tomohiko Usui, Department of Ophthalmology, Faculty of Medicine, University of Tokyo, 7-3-1 Hongo, Bunkyo-ku, Tokyo 113-8655, Japan; tomohiko-tky@umin.ac.jp.

Corneal neovascularization is a major sight-threatening condition and is caused by infections, inflammation, degenerative disorders, and long-time contact lens wear.[1] This major ocular complication can lead to corneal scarring, edema, lipidic deposition, and inflammation that may not only compromise visual acuity but also decrease the success rate of subsequent penetrating keratoplasty.[2] In the clinical setting, topical corticosteroids and nonsteroidal anti-inflammatory drugs (NSAIDs) remain the principal primary treatment for suppressing proliferating corneal vessels.[3] However, in corneas in which vessels have been established for extended periods, corticosteroid and NSAID treatment are ineffective. Although laser photocoagulation for corneal neovascularization has been reported,[4-7] this method achieves an inadequate effect because of the high incidence of recanalization and thermal damage to adjacent tissue.[4] The discovery of the many factors involved in corneal neovascularization and their mechanisms of action has been followed by efforts to develop new drugs specifically targeting these molecules. For example, therapy targeting vascular endothelial growth factor (VEGF) looks promising for the treatment of corneal neovascularization.[8] However, the agents tested thus far have yet to become available clinically.

Photodynamic therapy (PDT) has been introduced recently as a novel treatment for corneal neovascularization.[9] In this therapy, a photosensitizer (PS) is injected systemically and accumulates in newly formed vessels; it is then activated by mild laser excitement to liberate cytotoxic reactive oxygen species (ROS) that selectively occlude the target vessels. Although benzoporphyrin (verteporfin), a PS, is used for choroidal and corneal neovascularization clinically,[9] nonspecific binding activities of verteporfin induce skin phototoxicity in bright conditions, and patients must remain in the dark for 48 hours after injection of this drug. Hence, innovative PS should be developed for realizing safe and effective PDT.

Specific delivery of a PS to the neovasculature site might be a promising way to achieve safe and effective PDT for corneal neovascularization. Drug vehicles such as liposomes can be used for this purpose; however, the self-quenching effect of PS caused by aggregate formation could decrease the efficiency of ROS production. To solve this problem, we have recently developed dendrimer porphyrin (DP) as a novel PS for drug delivery (Fig. 1A).[10] It is assumed that the dendritic framework of DP might prevent the interactions of the center dye molecules, thereby achieving efficient ROS production even at extremely high concentrations. Indeed, encapsulation of DP into polymeric micelles (DP-micelle), which are characterized by the polyion complex core surrounded by poly(ethylene glycol) (PEG) palisades (Fig. 1C), resulted in remarkably increased photocytotoxicity.[11,12] We previously reported the review and general introduction of drug delivery of these PSs in corneal neovascularization.[13] In this study, to demonstrate the potential usefulness of DP and DP-micelle for PDT of corneal neovascularization, we investigated the accumulation of those PS

Investigative Ophthalmology & Visual Science, March 2008, Vol. 49, No. 3